OBJECT ENHANCEMENT AND EXTRACTION

Judith M. S. Prewitt

University of Pennsylvania
Philadelphia, Pennsylvania

INTRODUCTION

Object enhancement, extraction, characterization and recognition are closely linked aspects of visual perception, and cognizance of their interplay as well as their individual roles is important for the construction of successful image processing automata. The last two decades have produced a proliferation of models and computer realizations of sensory and cognitive processes in which both the degree of separation of these functions, and the manner of their integration, vary greatly. Past designs have been influenced heavily by practical considerations, and have tended to be simplistic. Only recently has technology advanced enough to permit unified consideration of all of these operations.

In early work in automated character recognition and aerial reconnaissance, object detection and recognition were often performed simultaneously. Images were either binary or high contrast, and consisted of standardized shapes or well defined curvilinear contours. Techniques for eliminating spurious noise in digitized images and for mending broken contours were either embedded in the recognition scheme (usually a variant of template matching), or else handled with a modicum of auxiliary processing. Objects of interest were identified with little or no explicit articulation. Surveys of this early work may be found in [127, 181, 202]. In approaches using representations such as Fourier transforms and Haar-Walsh expansions, the distinction between detection and characterization is also obscured, but these approaches have the advantage that no information is lost in the transformation from the original image domain to the domain of the representation, and objects can be resynthesized by inversion of the process [e.g., 2, 31, 49, 60, 227].

As attention turned toward less stylized scenes with greater tonal and topological information content, the distinction between sensory and cognitive processes was formalized. Feature extraction and object detection were considered precursors to description and identification. This division of function was harmonious with the modular viewpoint imposed by machine construction and programming. At the time, it was also the only practical approach to complex material [e.g., PR^2, OCR, 139].

When the potential of image-processing automata in scientific applications became evident, the relationship between reliable interpretation of visual material and image fidelity, long an acknowledged consideration in commercial communication systems, again became a compelling factor in design. Image restoration and enhancement research was revived principally because of interest in two areas: (1) video systems for terrestrial and extraterrestrial exploration, in which spatial and tonal degradations are unavoidable but almost completely reversible, and (2) systems for biomedical image processing, including quantitative scanning microscopy and interpretive medical radiography, in which object size is often at or near the limit of resolution, and anomalous imaging may result. In both cases, the resultant images are strongly dependent on the transfer function of the total electro-optical configuration, and proper image interpretation depends on correcting or compensating for degradation. Furthermore, the amount of data to be transmitted or stored is so great that optimal spatial and tonal quantization and efficient encoding became important considerations in data acquisition, and materially affected subsequent image manipulation [e.g., OEOIP, PPR, 222]. Image processors which were designed to handle these additional requirements still had a linear structure. They generally consisted of four types of independent units: transducer, preprocessor, feature extractor, and classifier; they performed signal detection, enhancement, object description, and identification, in that order.

Most recently, serious thought has been given to less trival pictorial material and scenes. Realistic complications include the following:

(1) fragmentation, coalescence, and disappearance of objects and object parts because of high noise levels and limited resolution;
(2) pseudo-resolution: the appearance of spurious objects and parts due to a singular relationship between the object and the transfer function of the transducer;
(3) differences in illumination, contrast, and signal to noise ratio over the field of view;

(4) variations in the amount of detail (high spatial frequency content) over the field of view;
(5) distortions due to the projective mapping from three to two dimensions;
(6) occlusion or overlapping of objects by others which intervene in the line of sight;
(7) eclipsing of objects by shadows;
(8) attenuation of high spatial frequencies, hence obliteration of fine detail and blurring of boundaries, because of phenomena such as glare, atmospheric turbulence, or fog;
(9) motion of object or sensor;
(10) ambiguity resulting from the use of a single function such as monochromatic reflectivity or transmissivity, which may be resolved by use of additional functions such as color and distance;
(11) intrinsic ambiguity due to uncertainty principle considerations.

Linear models cannot cope realistically with such complexities, and are being supplanted by models with cyclical or recursive structure, which can interleave detection and enhancement with parameterization and description, vary resolution, and change the focus or type of effort, so that tentative decisions and descriptions can be refined. This approach is implicit in many programs, albeit in rudimentary form. Such semi-formal heuristic models, as well as syntactic models, have been used in the analysis of noisy photomicrographs [20] and bubble chamber tracks [79, 169, 229, 231], in robot design [42, 59], and in the analysis of hand printing, handwriting and ill-formed printed text [57, 64, 122]. In these higher level models, the organized collection of information by primitive feature extractors, the assemblage of pictorial elements into objects, and the description of their relationships are all in accordance with explicit formulae for well formed scenes [98, 128, 129, 194].

Even with these complex models, the central and most difficult problem is characterization, i.e., extracting sets of significant features, properties, and relationships from a background of irrelevant detail. In most existing systems, a finite set of presumably robust and adequate features is preprogrammed. Insensitivity of individual feature extractors to noise and to acceptable variations in object size, registration, orientation, contrast, texture, and topological deformation is obviously desirable. On the other hand, redundancy in ensembles of feature extractors and object characterizers is wasteful and can actually dilute measurement of overall discriminatory achievement [165, 170]. Criteria exist for the deletion of irrelevant or uninformative features and the optimal utilization of informative features [170, 211, 228], and there are some results on the theoretical limitations of certain popular discrimination techniques [130]. Little guidance is available, however, on the generation of suitable new features [for exceptions, see 217]. Thus the success of current systems depends basically on the intuition and ingenuity of the programmer and designer.

This paper is concerned with accomplishments in these difficult tasks of feature and object extraction and enhancement. An enormous amount of research has been done in the last 25 years, but reports are scattered throughout the literatures of several disciplines. Although collected readings, conference proceedings, and surveys have appeared from time to time, little of this diverse material has been unified (until the recent appearance of [183]) and evaluated. Rather than aim for complete and definitive coverage, we have set the more modest goal of presenting basic principles with illustrative implementations.

Image formation may be described mathematically in terms of degradation operators or spread functions which characterize the optical communication channel. Image processing in turn can be thought of as modification or transformation of the image by (1) restoration operators, (2) enhancement operators, (3) structural operators or feature extractors, and (4) syntactic schemata. The basis of this classification is function; a given operator may be used in several capacities.

Restoration operators compensate for the system spread function and other noise and permit reconstruction of the object signal. Degradation and restoration are thus inverse operations. Enhancement operators change the image further rather than restore it—directly, by masking or convolution, or indirectly, by emphasizing or deemphasizing the spatial frequency and tonal content. Both restoration and enhancement may be used as aids to either human or automatic photointerpretation.

Structural operators detect picture elements such as contours, features and connected regions. Syntactic schemata direct the concatenation or assemblage of picture elements into figures and more complex configurations; in our sense they are higher level, organizational procedures.

In the body of this paper, we shall discuss the use of such operators for object enhancement and detection. A paper on object recognition and on syntactic schemata is in preparation.

IMAGE FORMATION

Image formation involves a spatial reorganization of the irradiance pattern of an object by a process that is not one to one, so that the recorded image is at best a degraded copy of the original. The information content of the recorded image is limited by the resolution of the imaging system and by the presence of both random and systematic noise. Whether restoration and other enhancement processes are warranted or even possible in any particular case depends on the transfer characteristics of the imaging system and also on the purpose for which the image was recorded.

The mathematical theory of integral transformations is a suitable framework for describing many aspects of image formation, restoration, enhancement, and object detection. The integral transform $F(\omega)$ of a function $f(r)$ is defined by an equation of the form

$$F(\omega)=\int_{\alpha}^{\beta} f(r)K(\omega,r)dr$$

where $K(\omega,r)$ is a specific function of r and ω called the kernel of the transform. The variables r and ω may be real or complex numbers or vectors, and the limits of integration α and β may be finite or infinite. If the kernel $K(\omega,r)$ and the transform $F(\omega)$ are known, then the process of determining a solution $f(r)$ of the integral equation is called inversion. The properties of the original function f and the kernel K over the region of integration determine the existence of the integral transform F and the existence of (unique) inversion formulae or algorithms giving f as an integral transform of F:

$$f(r)=\int_{\alpha'}^{\beta'} F(\omega)K^{-1}(\omega,r)d\omega$$

Mathematical conditions are detailed elsewhere; they are presumably satisfied for the cases under discussion here, but should be verified in specific applications [31, 205, 214, 237].

In using this formalism to describe two-dimensional image formation, the function itself represents the object pattern, the kernel represents the action of the imaging system, and the transform gives the resultant image. The kernel may be thought of as a blurring operator or spread function s, which modulates and combines intensity values at all luminous points on the original object o, and thereby forms the image:

$$i = s ** o$$

$$i(x,y) = \int_{-\infty}^{\infty}\int_{-\infty}^{\infty} o(\xi,\eta)\, s(x,y,\xi,\eta)\, d\xi\, d\eta$$

Restoration is mathematically equivalent to finding the appropriate inversion formula

$$o = s^{-1} ** i$$

$$o(\xi,\eta) = \int_{-\infty}^{\infty}\int_{-\infty}^{\infty} i(x,y)\, s^{-1}(x,y,\xi,\eta)\, dx\, dy$$

The imaging process is schematized in Fig. 1. See [108, 121, 153].

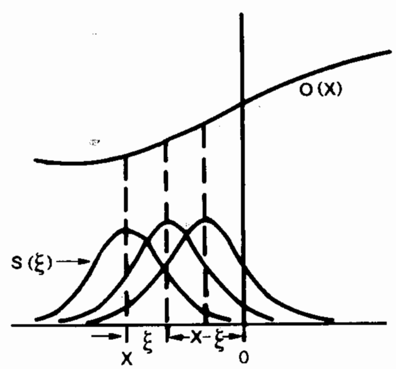

Figure 1. The imaging process. The amplitude at any point in the image is built up from contributions associated with all luminous points in the object. This is described mathematically by the convolution of an object o(x) with a spread function s(ξ). After Perrin [153].

Image processing operations such as enhancement can also be represented within this framework. If o is the original pattern and Ω is the processing operator, then $p = \Omega o$ or $p(x, y) = [\Omega o](x, y)$ represents the processed pattern. Shifting the original pattern is described by translation operators

$$[T_{\xi\eta} o](x,y) = o(x-\xi, y-\eta)$$

and uniform amplification is described by scaling operators

$$[c_k o](x,y) = k \cdot o(x,y)$$

Most operators in current use satisfy the following criteria:

(a) Ω is homogeneous or position invariant, i.e., it commutes with all translation operators

$$\Omega T_{\xi\eta} = T_{\xi\eta} \Omega$$

(b) Ω is linear, i.e., it commutes with all scaling operators and satisfies a superposition theorem

$$\Omega c_k = c_k \Omega \quad \text{and} \quad \Omega(o_1 + o_2) = \Omega o_1 + \Omega o_2$$

(c) Ω is local, i.e., $[\Omega o](x,y)$ depends only on the values of o in a specified neighborhood of the point (x,y) where N(x,y) is obtained by translating a neighborhood N of the origin

$$N(x,y) = \{(x',y') \mid (x-x', y-y') \in N\}$$

Some operators also satisfy

(d) Ω is isotropic, i.e., rotation and reflection invariant.

In these cases a large body of mathematical theory becomes applicable to image processing [48, 149]. It is well known that any homogeneous linear operator Ω is equivalent to a convolution integral, in which the kernel is a function of two displacements rather than four spatial coordinates, and conversely:

$$s(x,y,\xi,\eta) = s_1(x-\xi, y-\eta)$$

Thus, to each such operator Ω there corresponds a kernel function s_Ω which allows us to describe the action of Ω on all functions f in its domain as a convolution integral:

$$\Omega f = s_\Omega ** f = f ** s_\Omega$$

$$\text{or } [\Omega f](x,y) = \iint f(\xi,\eta)\, s_\Omega(x-\xi, y-\eta)\, d\xi\, d\eta = \iint f(x-\xi, y-\eta)\, s_\Omega(\xi,\eta)\, d\xi\, d\eta$$

Conversely, any such convolution integral is a homogeneous linear operator.

In systems where degradation is virtually independent of location, image formation itself can be described using a convolution integral:

$$i = o ** s = s ** o$$

$$\text{or } i(x,y) = \int_{-\infty}^{\infty}\int_{-\infty}^{\infty} o(\xi,\eta)s_1(x-\xi,y-\eta)\,d\xi d\eta$$
$$= \int_{-\infty}^{\infty}\int_{-\infty}^{\infty} o(x-\xi,y-\eta)s_1(\xi,\eta)\,d\xi d\eta$$

The kernel of this integral is called the point spread function. Furthermore, the result of applying any homogeneous linear operator Ω to the blurred picture i can be expressed in terms of a modified spread function $\hat{s}=\Omega s$ as follows:

$$\hat{i} = \Omega i = \Omega(so) = (\Omega s)o = \hat{s}o$$

In practice, the spread function is essentially a local operator and the limits of integration become finite. In some cases, the degradation is also isotropic or direction independent, the corresponding circularly symmetric spread function has the form

$$s_1(x-\xi,y-\eta) = s_2(r)$$

and additional simplification of the equations is possible through the use of polar coordinates:

$$x-\xi = r\cos\theta$$

$$y-\eta = r\sin\theta$$

Restoration is the inverse convolution

$$s^{-1}(x,y,\xi,\eta) = s_1^{-1}(x-\xi,y-\eta)$$

Given a processing kernel Φ, it is sufficient to know the effect of Φ on the inverse spread function, since

$$\Phi o = \Phi(s_1^{-1}i) = (\Phi s_1^{-1})i$$

Most useful in image processing are those linear integral transforms for which there are "convolution-product" and "inversion" theorems. For such a distinguished kernel, if f and g are arbitrary functions whose integral transforms are

$$T[f] = F \quad \text{and} \quad T[g] = G$$

respectively, then the integral transform of the convolution of f and g is found by multiplication:

$$T[f ** g] = T[f]T[g]$$

Furthermore,

$$T^{-1}[FG] = f ** g$$

Also in extensive use are two operations derived from convolution, the cross correlation and autocorrelation, which measure goodness of match or fit of two patterns. Let $\bar{f}$ be the result of reflecting f in the origin:

$$\bar{f}(x,y) = f(-x,-y)$$

The cross correlation $f \times g$ is defined by

$$f \times g = f ** \bar{g} = \int\int g(\xi-x,\eta-y)f(\xi,\eta)\,d\xi d\eta$$
$$= \int\int g(\xi,\eta)f(\xi+x,\eta+y)\,d\xi d\eta$$

and the autocorrelation $f \times f$ is defined by

$$f \times g = f ** \bar{f}$$

Symmetry and antisymmetry properties of these correlations make them useful in image analysis:

$$\overline{f ** g} = \bar{f} ** \bar{g}$$

$$\overline{f \times g} = g \times f$$

Convolution and inversion theorems are known for several kernels, such as the Laplace and Mellin transforms, but the Fourier and Hankel transforms have been the most useful in object detection and enhancement for several reasons: first, they can readily be interpreted in terms of spatial frequency; second, they can be implemented efficiently by digital as well as electro-optical and optical means [27, 28]. Two-dimensional moments [1, 86] and transforms involving Haar-Walsh functions [51, 118] and Chebyshev polynomials [198] have also been used.

The complex Fourier transform T[f] of a univariate function is defined by

$$F(\omega) = \frac{1}{\sqrt{2\pi}}\int_{-\infty}^{\infty} f(r)e^{i\omega r}\,dr$$

and the corresponding inverse transform $T^{-1}[F]$ is given by

$$f(r)=\frac{1}{\sqrt{2\pi}}\int_{-\infty}^{\infty}F(\omega)e^{-ir\omega}d\omega$$

$F(\omega)$ is generally complex valued with real and imaginary parts comprising the cosine and sine transforms

$$\operatorname{Re}F(\omega)=\frac{1}{\sqrt{2\pi}}\int_{-\infty}^{\infty}f(r)\cos\omega r\,dr$$

$$\operatorname{Im}F(\omega)=\frac{1}{\sqrt{2\pi}}\int_{-\infty}^{\infty}f(r)\sin\omega r\,dr$$

Related to these is the power spectrum Pow[f] defined by

$$P(\omega)=F(\omega)F(\omega)^{*}=\operatorname{Re}^2F(\omega)+\operatorname{Im}^2F(\omega)$$

where * denotes complex conjugation. For functions of two variables, the transform $T[f]$ and the inverse transform $T^{-1}[F]$ are defined by

$$F(s,t)=\frac{1}{2\pi}\int_{-\infty}^{\infty}\int_{-\infty}^{\infty}f(x,y)e^{i(sx+ty)}dxdy$$

$$f(x,y)=\frac{1}{2\pi}\int_{-\infty}^{\infty}\int_{-\infty}^{\infty}F(s,t)e^{-i(xs+yt)}dsdt$$

The Fourier transform satisfies the invertibility theorem

$$T^{-1}[T[f]]=f$$

the linearity or superposition theorem

$$T[\alpha f+\beta g]=\alpha T[f]+\beta T[g]$$

the symmetry-antisymmetry theorem

$$T^{-1}[\bar{f}]=T[f]$$
$$T^{-1}[f^{*}]=T[f]^{*}$$

the shift and rotation theorem

$$T[f(x+x_0,y+y_0)]=e^{-i(sx_0+ty_0)}F(s,t)$$
$$T[f(x,y)e^{i(s_0x+t_0y)}]=F(s+s_0,t+t_0)$$

the product-convolution theorem

$$T[g**h]=T[g]T[h]$$
$$T^{-1}[T[g]T[h]]=g**h$$

and the Wiener-Khinchin theorem on power spectra

$$T[f\times f]=T[f]T[f]^{*}=P[\omega]$$

The Hankel transform enters naturally in the analysis of systems with isotropic point spread functions and greatly facilitates restoration. The Hankel transform of order n is defined by

$$H_n[f]:F_n(\omega)=\int_0^{\infty}rf(r)J_n(\omega r)dr$$

where $J_n(z)$, the nth order Bessel function, has the integral representation

$$J_n(z)=\frac{1}{\pi}\int_0^{\pi}\cos(z\cos\phi-n\phi)d\phi=\frac{1}{2\pi}\int_{-\pi}^{\pi}e^{iz\sin\theta-in\phi}d\phi$$

In particular,

$$J_0(z)=\frac{1}{2\pi}\int_{-\pi}^{\pi}e^{iz\cos(\theta-\alpha)}d\theta \qquad (\alpha\ \text{arbitrary})$$

The Hankel transform has circular symmetry and satisfies scaling and convolution theorems, and has a particularly simple inversion formula:

Scaling: $H[f(\alpha r)](\omega)=\frac{1}{\alpha^2}H[f(r)](\omega/\alpha)$

Convolution: $H[f**g]=H[f]H[g]$

where $f**g=\int\int f(\sqrt{\xi^2+\eta^2})g(\sqrt{(x-\xi)^2+(y-\eta)^2})d\xi d\eta$

Inversion: $HH[f]=f$

By changing from rectangular to polar coordinates,

$$x=r\cos\theta \qquad s=\omega\cos\phi$$
$$y=r\sin\theta \qquad t=\omega\sin\phi$$

any function f and its two-dimensional Fourier transform F become

$$f(x,y)=f_o(r,\theta)=\frac{1}{2\pi}\int_0^{\infty}\omega d\omega\int_0^{2\pi}F_o(\omega,\phi)e^{-ir\omega\cos(\theta-\phi)}d\phi$$

$$F(s,t)=F_o(\omega,\phi)=\frac{1}{2\pi}\int_0^{\infty}rdr\int_0^{2\pi}f_o(r,\theta)e^{i\omega r\cos(\theta-\phi)}d\theta$$

If f has circular symmetry

$$f(x,y)=f_o(r,\theta)=f(r)=f(\sqrt{x^2+y^2})$$

then the direct and inverse Fourier transforms reduce to the simpler, univariate, Hankel transform

$$F_o(\omega,\phi)=\frac{1}{\pi}\int_0^{\infty} rf(r)\left[\int_0^{2\pi}\cos(\omega r\cos\phi)d\phi\right]dr$$
$$=\int_0^{\infty} rf(r)J_0(\omega r)dr=F_1(\omega)=H_0[f]$$
$$f(r)=\int_0^{\infty}\omega F_1(\omega)J_0(r\omega)d\omega=H_0[F_1]$$

Analogous sine, cosine and Hankel transforms can be defined when the limits of integration are finite rather than infinite, and appropriate inversion formulas can be derived [200]. For example, the finite sine-cosine transforms are identical to the coefficients of the ordinary Fourier series; the inverse is the series itself.

$$F(\omega)=\int_0^{\pi} f(x)\cos\omega x\,dx \qquad (\omega \text{ an integer } >0)$$

The finite Hankel transform is defined by bounding the range of integration:

$$H(\omega)=\int_0^1 f(r)rJ_n(\omega r)dr$$

where ω is a positive root of $J_n(\omega)=0$. By the theory of Fourier-Bessel series [31], $f(r)$ can be represented by a Bessel series in the range $0\leq r<1$:

$$f(r)=\sum_{\omega} a_\omega J_n(\omega r)$$

where the coefficients are

$$a_\omega=\frac{2}{J^2_{n+1}(\omega)}\int_0^1 f(r)rJ_n(\omega r)dr=2H(\omega)/J^2_{n+1}(\omega)$$

Hence the inversion formula for the finite Hankel transform is

$$f(r)=2\sum_{\omega>0,\,J_n(\omega)=0} F(\omega)J_n(\omega r)/J^2_{n+1}(\omega)$$

Since real world images and spread functions have limited spatial extent, these finite transforms may be more relevant for picture processing.

IMAGE RESTORATION

Efforts to extract features or objects can be in vain when there is severe distortion of the image. What is enhancement in one application may be a hindrance in others. Corrections needed in preparation for quantitative image analysis may be entirely superfluous for qualitative visual perception. If the nature of the degradation can be determined in advance, either from theory or by using known test objects to calibrate the imaging system, then corrective measures can be applied to new images as warranted.

Degradation may be caused by system dependent or object dependent factors, which can generally be classified into (1) deterministic factors, including (a) distortions of the spatial coordinate system and the photometric scale, and (b) blurring, which can be described as convolution with some point spread function; and (2) additive stochastic noise which is superimposed either before or after imaging.

Restorative procedures can also be classified according to the type of degradation to which they are addressed. Specific techniques include: (1) construction of tables of corrections and interpolating functions; (2) inversion of integral transforms; and (3) optimal filters for minimizing the mean square error of reconstruction or for maximizing the signal to noise ratio. Many of the concepts connected with restoration are also relevant to nonrestorative image enhancement (e.g., sharpening) and feature detection.

Rectification of geometric distortion and photometric errors which are spatially and temporally stable (e.g., consistent slanting of lines; fixed but uneven illumination) involves changing coordinates and brightness values throughout the image. Corrections can be tabulated for selected points and suitable interpolation formulas used at intermediate points, or they can be summarized in the form of fitted functions.

Displacements for straightening the image coordinate raster can be obtained using a two-dimensional test grid. Photometric errors can be corrected by using the results for uniformly illuminated test fields, or the correction can be provided pointwise, on-line, in the form of a compensating reference signal. In most cases, the restoration involves nonlinear, position dependent operations [120, 143].

Most methods of restoration and enhancement involve homogeneous linear operators for which convolution-product or inversion theorems hold. From a mathematical point of view, any invertible operator will suffice. Since imaging is a convolution, the object, image, and spread function transforms are related by

$$F[i]=F[s{*}{*}o]=F[s]F[o]$$

Formally, the restored picture is obtained by reinverting,

$$F[o]=F[i]/F[s]$$
$$o=F^{-1}[F[i]/F[s]]=F^{-1}F[i]{*}{*}F^{-1}[1/F[s]]$$

a technique that is often unsatisfactory because the reciprocal $1/F[s]$ is singular, the ratio $F[i]/F[s]$ is indeterminate or undefined, or the restored image will be heavily contaminated by restored noise.

The main steps in applying inversion methods to restorative enhancement are: selection of an appropriate integral transform (kernel), determination of the transform of the spread function, and inversion of its reciprocal. The transform of the spread function depends only on the relationship of the latter to the selected kernel, and in principle it can be determined by using any convenient object-image pair:

$$1/F[s]=F[o]/F[i]$$

Points, slits or lines, and especially edges, are the simplest and most widely used test objects.

If objects are thought of as mass distributions over the x-y plane, then the response of the imaging system can be described [148] in terms of two-dimensional line impulses or generalized Dirac delta functions $\delta[\alpha(x,y)]$ representing a mass distribution of density

$$\lambda(x,y)=[(\partial\alpha/\partial x)^2+(\partial\alpha/\partial y)^2]^{-1/2}$$

along the curve $\alpha(x,y)=0$.

Point masses located at the intersection of two curves $\alpha_1(x,y)=0$ and $\alpha_2(x,y)=0$ are described by

$$\delta[\alpha_1(x,y)]\delta[\alpha_2(x,y)]=\sum_{\alpha_1(x_1,y_1)=\alpha_2(x_1,y_1)}\frac{\delta(x-x_1)\delta(y-y_1)}{|\alpha_{1x}\alpha_{2y}-\alpha_{1y}\alpha_{2x}|}$$

in which the elementary impulses $\delta(x-x_1)$ and $\delta(y-y_1)$ represent impulse distributions on the lines $x=x_1$ and $y=y_1$. For a given degradation operator Ω, the value of the point spread function (PSF) $s_\Omega(x,y)$ itself gives the response to a point mass located at $x=x_0$, $y=y_0$:

$$PSF_\Omega(x,y)=\iint s_\Omega(u,v)\delta(x-u)\delta(y-v)\,du\,dv$$

while the image corresponding to a uniform object $o=c$ is also uniform:

$$k_\Omega(x,y)=k_\Omega=c\iint s_\Omega(x-u,y-v)\,du\,dv=c\iint s_\Omega(u,v)\,du\,dv$$

The response to a line impulse situated on the y-axis is the vertical line spread function (LSF):

$$LSF_\Omega(x,y)=h_\Omega(x)=PSF_\Omega(x,y){*}{*}\delta(y)=\int_{-\infty}^{\infty}s_\Omega(x,y)\,dy$$

and the result for a straight edge similarly oriented ($o=0$ in the left half plane and 1 in the right half plane) is called the vertical edge spread function (ESF) or edge trace

$$ESF_\Omega(x,y)=g_\Omega(x)=\int_0^\infty LSF_\Omega(x-u,y)\,du=\int_0^\infty h_\Omega(x-u)\,du$$
$$=\int_{-\infty}^{x}h_\Omega(u)\,du$$

Formally, the LSF is the derivative of the ESF

$$LSF_\Omega(x)=dESF_\Omega(x)/dx$$

Degradation and restoration have customarily been analyzed using the Fourier transform. The output and image transform,

$$F[o](u,v)=O(u,v)=\iint o(x,y)e^{-i(ux+vy)}\,dx\,dy$$

and

$$F[i](u,v)=I(u,v)=\iint i(x,y)e^{-i(ux+vy)}\,dx\,dy$$

are related via the complex valued system transfer function

$$F[s]=F[i]/F[o]=\iint s(x,y)e^{-i(ux+vy)}\,dx\,dy$$

In vector notation

$$\vec{\omega}=iu+jv \qquad \vec{r}=ix+jy$$
$$\omega^2=u^2+v^2 \qquad r^2=x^2+y^2$$

the complex transfer function is written as

$$M(\vec{\omega})=M(u,v)=F[s](u,v)=\iint s(\vec{r})e^{-i(\vec{\omega}\cdot\vec{r})}d\vec{r}$$

The real component is equal to the cosine transform, and the imaginary component to the negative sine transform of the vertical and horizontal LSF's

$$M(u,v)=\iint s(x,y)dy \cos ux\, dx - i\iint s(x,y)dx \sin vy\, dy$$
$$=\cos[LSF(x)](u) - i \sin[LSF(y)](v)$$

The complex transfer function is usually replaced by the real valued transform pair consisting of the modulation transfer function (MTF)

$$MTF(\vec{\omega}) = (F[s]F[s]^*)^{1/2} / \iint s(\vec{r})d\vec{r}$$
$$= \sqrt{\cos^2[LSF(x)]u + \sin^2[LSF(y)](v)} / \iint s dr$$

and the phase transfer function (PTF)

$$PTF(\vec{\omega}) = \arctan \frac{F[s]-F[s]^*}{F[s]+F[s]^*} = \frac{\operatorname{Im} F[s]}{\operatorname{Re} F[s]}$$

Thus we can write the complex transfer function as

$$M(\vec{\omega}) = MTF(\vec{\omega})e^{iPTF(\vec{\omega})}$$

These transfer functions are readily interpreted in terms of the sine wave response, i.e., the result of imaging a bar pattern with sinusoidally varying intensity. Such an input with mean intensity a_o, spatial frequency or repetition rate ω and associated amplitude a_ω,

$$o(x,y) = o(x) = a_o + a_\omega \cos 2\pi\omega x$$

is transformed into a similar output with unaltered spatial frequency, but amplitude and phase changed as follows:

$$i(x,y) = a_o k_\Omega + a_\omega(\cos 2\pi\omega x\, C_\Omega(\omega) + \sin 2\pi\omega x\, S_\Omega(\omega))$$
$$= a_o k_\Omega + a_\omega(\cos 2\pi\omega x - \Phi_\Omega(\omega))|M_\Omega(\omega)|$$

where

$$C_\Omega(\omega) = \int LSF(u) \cos 2\pi\omega u\, du$$
$$S_\Omega(\omega) = \int LSF(u) \sin 2\pi\omega u\, du$$
$$M_\Omega(\omega)^2 = C_\Omega(\omega)^2 + S_\Omega(\omega)^2$$
$$\Phi_\Omega(\omega) = \arctan(S_\Omega(\omega)/C_\Omega(\omega))$$

Here k_Ω is the (de)intensified value of the constant field, while $C_\Omega(\omega)$ and $S_\Omega(\omega)$ are the cosine and sine transforms of the LSF. The MTF

$$MTF_\Omega(\omega) = (C_\Omega(\omega)^2 + S_\Omega(\omega)^2)^{1/2}/k_\Omega$$

gives the attenuation of amplitude, while the PTF

$$PTF_\Omega(\omega) = \arctan(S_\Omega(\omega)/C_\Omega(\omega))$$

gives the displacement of phase. Under fairly general conditions (absolute integrability), a two-dimensional function can be decomposed into sinusoidal components and similar expressions can be developed for their spectra.

Mertz and Gray [123] give an extensive analysis, using Fourier techniques, of two-dimensional picture scanning and transmission. They include discussions of blurring due to optical system limitations, and of superposition of extraneous patterns not present in the original, due to singular object-scanner relationships. Perrin [153] gives a qualitative discussion of the same concepts.

Fig. 2 illustrates image formation for a sinusoidal input of spatial frequency ω and finite PSF of width d, as a function of the ω-d relationship. Fig. 3 shows how the shape of the spread function affects imaging. Fig. 4 shows a simple case of anomalous imaging.

Imaging is fully described by the complex valued transform pair, which in turn is determined by either the PSF or LSF. The PSF is also involved in restoration calculations. However, because suitable test objects are lacking, it is usually more difficult to determine it by experiment than to determine the LSF's, and indirect determination is needed. In general, the PSF can be found indirectly, provided that its convolution PSF ** $\delta[\alpha x+\beta y=0]$ with line impulse functions is known for all orientations of a line $\alpha x+\beta y=0$.

These formidable requirements are weakened if the degradation corresponds to a circularly symmetric spread function; one LSF alone is then sufficient [93]. We have seen that the Fourier transform of an isotropic PSF, $s(\vec{r}) = s(r)$, is a Hankel transform

$$H(\omega) = 2\pi \int_0^\infty s(r) J_0(\omega r) r\, dr = H(\sqrt{u^2+v^2})$$

where $J_0(z)$ is the Bessel function of the first kind and zero order. It is readily verified that the PTF vanishes, so that the complex transfer function reduces to an ordinary MTF

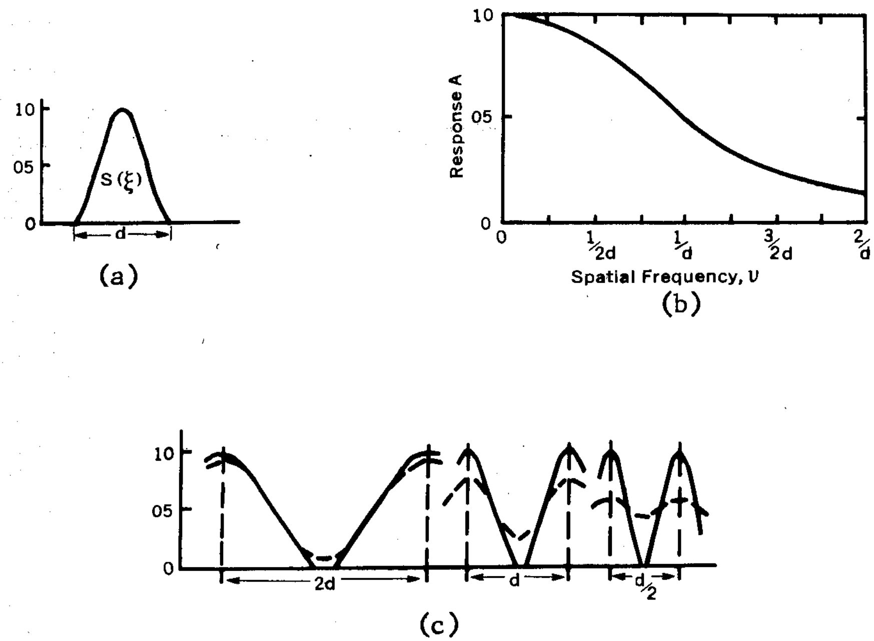

Figure 2. Image formation for a sinusoidal input: (a) hypothetical PSF of width d; (b) response to spatial frequency ν (measured in units of 1/d); (c) image functions (dotted) corresponding to sinusoidal object functions (solid) of spatial frequencies 1/2d, 1/d, and 2/d. After Perrin [153].

$$M(\vec{\omega})=\int_{-\infty}^{\infty}LSF(x)e^{-i\omega x}dx=2\int_{0}^{\infty}LSF(x)\cos\omega x dx=MTF(\sqrt{u^2+v^2})$$

Further, if the Hankel inversion can be performed, the spread function is recoverable as

Figure 3. Anomalous imaging effects showing the limitations of the MTF as a descriptor of resolution: (a) two hypothetical spread functions with different imaging properties; (b) edge traces for the spread functions in (a); (c) corresponding modulation transfer functions; (d) as measured by the MTF, the peaked function b compromises detail more than does the bell curve a, but b is better than a in resolving two point sources. After Perrin [153].

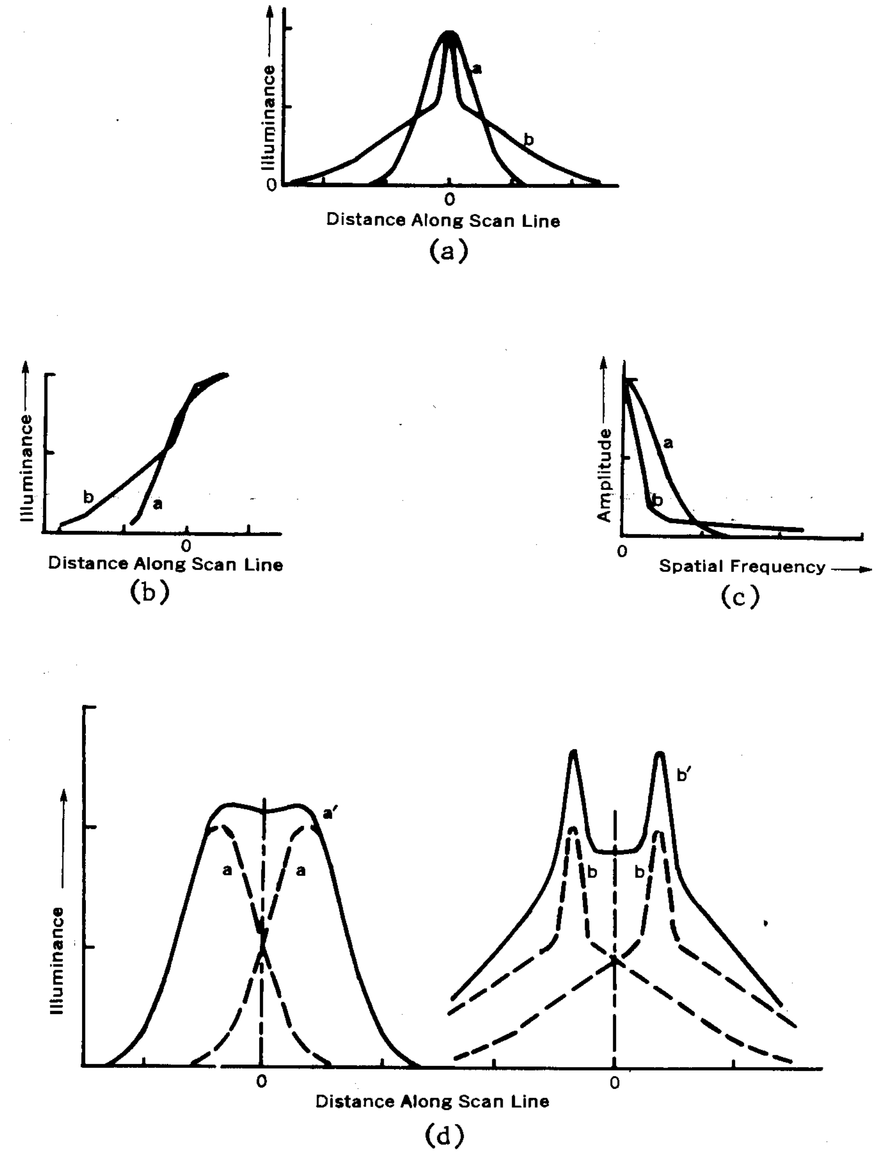

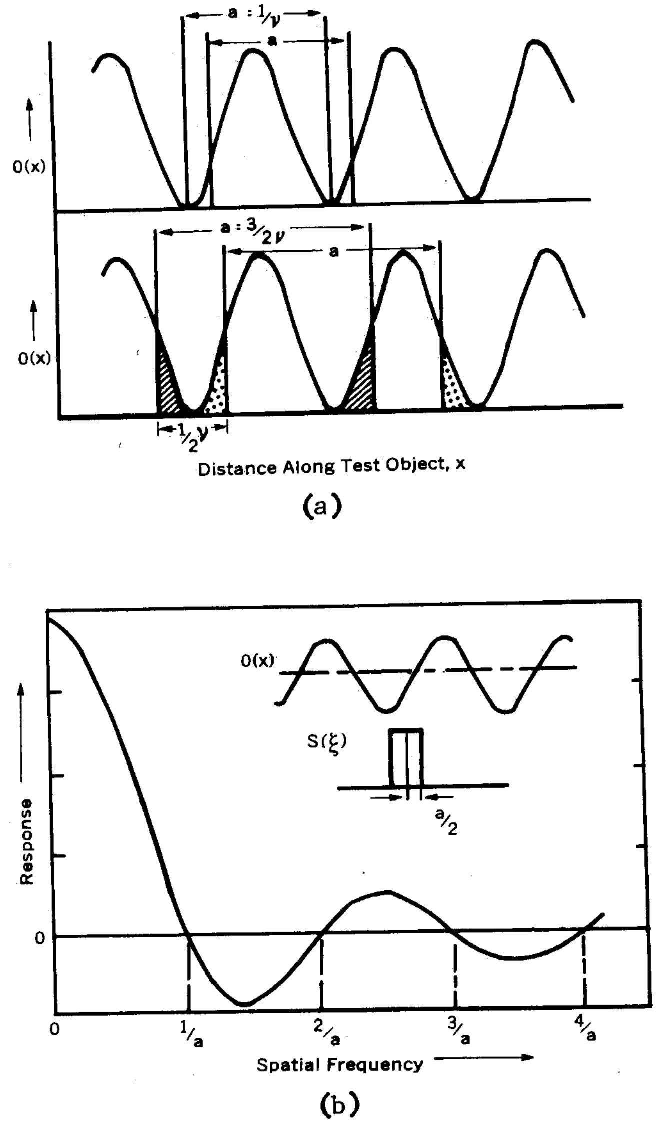

Figure 4. A simple case of anomalous imaging: (a) when a sine wave pattern of width d is imaged by a square wave spread function of the same width, the image is uniform; (b) when the spread function is wider, extraneous patterns are created, causing the phenomenon of pseudoresolution. After Perrin [153].

$$S(\vec{r}) = S(r) = \frac{1}{2\pi}\int_0^\infty M(\omega)J_0(\omega r)\omega\, d\omega$$

As an example, Rao and Jain [171] have derived MTF's for symmetric gaussian and exponential functions.

To make practical use of these ideas, numerical analysis can be used to estimate the spread function from regularly spaced photometric samples of an edge trace, based on the observation that the LSF is the derivative of the ESF. The ESF is estimated by least squares trigonometric approximation of the edge trace, and the LSF is estimated from this by direct differentiation [182]. The MTF and PTF for the isotropic case can then be approximated by taking sine and cosine transforms. Taking this one step further, the PSF can be gotten from the MTF by numerical integration. Errors can be ascertained for each computation (also see [162, 223]).

Given these pertinent quantities, operations can be implemented either directly, in the spatial (x-y) domain, or indirectly, in the frequency (u-v) domain. The indirect method consists of multiplying the Fourier transform of the picture with a corrective filter 1/MTF in the frequency domain, and then reinverting the resultant compensated spectrum back to the spatial domain. In the direct method, the picture is convolved in the original spatial domain with a mask gotten by inverting this corrective filter. The direct method has long been used for digital implementations. The indirect method (spatial frequency filtering) has been preferred in analog systems, but since the development of the fast Fourier transform [3, 29, 152] it is reasonable to use it for digital processing as well.

In terms of the Fourier transform, restoration

$$o(x,y) = \iint i(\xi,\eta)s^{-1}(x-\xi, y-\eta)\,d\xi d\eta$$

is achieved by applying the operator

$$s^{-1}(x,y) = \iint (1/F[s](u,v))\,e^{i(ux+vy)}\,du\,dv$$

where F[s] is the transform of the spread function. As we have just seen, recovery from isotropic degradation involves just the ordinary MTF and the operator simplifies to a Hankel transform of 1/MTF

$$s^{-1}(x,y) = \iint_{-\infty}^{\infty} (1/\mathrm{MTF}(\sqrt{u^2+v^2}))\,e^{i(ux+vy)}\,du\,dv$$
$$= 2\pi\int_0^\infty (1/\mathrm{MTF}(\omega))J_0(\omega)r\,dr$$

Practical and theoretical difficulties limit the applicability of this convolution-inversion approach. The picture may be complicated by superimposed stochastic noise, or the degradation may be anisotropic, and require more than the ordinary MTF. The method will also fail to give perfect restoration whenever the quotient $F[i]/F[s]$ becomes either infinite or indeterminate. Modifications have been proposed to make this a feasible, albeit imperfect, method of restoration and several more realistic alternatives have been suggested as well.

When the spectrum of superimposed noise and the object spectrum are fairly distinct, as is the case with systematic noise (where the frequencies associated with noise cluster in the spatial frequency domain), or with high frequency noise and a low frequency object, a truncated MTF is useful. For noise centered around discrete frequencies, sharply peaked filters are appropriate. But if they are too broad they will also remove picture information, and if too sharp they will leave residual noise. Examples of such filters are square and triangular truncations of the cosine:

$$\operatorname{sinc} 2\pi(\omega-\omega_0)f = \frac{\sin 2\pi(\omega-\omega_0)f}{2\pi(\omega-\omega_0)f}$$

and

$$\operatorname{sinc}^2 2\pi(\omega-\omega_0)f$$

where f is a cutoff sharpness parameter. Periodic systematic noise can be detected by cross correlation with sinusoids, and subtractive correction can be applied to the image.

In cases where it is desirable to avoid overemphasis of high frequencies or to suppress singularities of a band limited MTF, a cutoff frequency Ω_0, determined by the characteristics of the object and the noise, is chosen so that noise enhancement will not defeat image enhancement. A modified system MTF defined by

$$\begin{aligned} \text{modified MTF}(\omega) &= \text{MTF}(\omega) && \text{if } \omega<\omega_{max} \\ &= \text{constant} >0 && \text{if } \omega\geq\omega_{max} \end{aligned}$$

is inverted and convolved with the picture. Instead of the ideal flat frequency response, the actual response is level up to the cutoff frequency and then tapers off. This correction can also be made contextual, by turning the filter off at points of high contrast detail where the local differences in brightness exceed a threshold [13, 116, 143].

If some extraneous information or residual degradation is tolerable in the recovered image, compromise processors can often be found. Let o, i and p represent original object, degraded image, and processed picture, respectively. If the system spread function s_{IN} is known, and if a final response spread function s_{OUT} can be specified after considering a prototype image and an acceptable processed version, then the desired processing spread function s_{PROC} is given by

$$s_{OUT} = s_{IN} ** s_{PROC}$$

and its Fourier transform by

$$F[s_{PROC}] = F[s_{OUT}]/F[s_{IN}]$$

The processed picture

$$\begin{aligned} p = i ** s_{PROC} &= o ** s_{OUT} \\ &= F^{-1}(F[i]F[s_{PROC}]) \\ &= F^{-1}(F[i]F[s_{OUT}]/F[s_{IN}]) \end{aligned}$$

can be compared with a perfect restoration

$$o = F^{-1}(F[i]/F[s_{IN}])$$

As Fig. 5 indicates, for any specific operation the existence of the desired compromise processor must be verified. For example, a square PSF acting on a line (delta function) object produces a square wave input image with corresponding input MTF equal to sinc ($k\omega$). If a line output is demanded, the response PSF must also be a delta function, with a flat MTF. The required processor has MTF equal to 1/sinc ($k\omega$), a function which has unrealizable infinities. On the other hand, if a centrally restored image with accompanying low-intensity ghosts is acceptable, the desired output MTF is $\sin^2 \omega f$ and the required processor spectrum $\omega f \sin \omega f$ is realizable [68].

In principle, we can reconstruct the Fourier transform of an object wherever the spread function transform does not vanish. In practice, however, there is a cutoff frequency ω_0 defining a forbidden region in which the transform does indeed vanish. The reconstruction based on the truncated MTF is band limited and, at best, imperfect. The use of

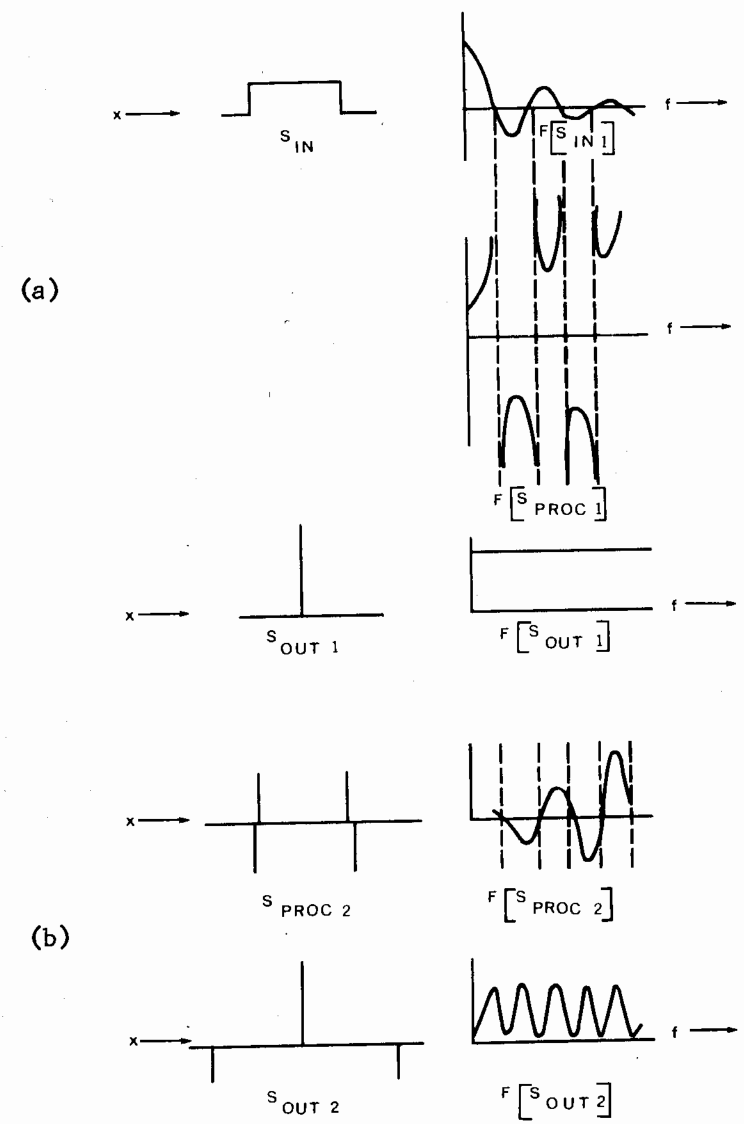

Figure 5. The use of substitute processors: (a) the restoration processor cannot be realized; (b) the compromise processor, which produces faint ghosts, can be implemented. After Harris [68].

substitute processors by definition gives a deficient but nevertheless acceptable picture. When such methods of compensation fail, more sophisticated methods must be used.

It has been shown that perfect digital reconstruction of two-dimensional objects can be accomplished in the absence of noise, with two provisos: (1) that the object is limited in spatial extent, and (2) that experimental knowledge of the image and the PSF is available [12, 45, 196, 197]. Under these conditions, the integral imaging equation can be solved for the object in terms of the image. The solution is expressed as a series expansion in the eigenfunctions and eigenvalues of the system spread function. The eigenfunctions can be interpreted as objects that are only scaled and translated by the imaging system. The expansion can be performed in the object domain or in the frequency domain. In both cases, certain higher transcendental functions are involved; these are the radial and angular prolate spheroidal wave functions. In the object domain

$$o(x)=\sum_{n=0}^{\infty}\int_{-\alpha}^{\alpha}(\sigma_n(x)\sigma_n(\xi)/\lambda_n)i(\xi)d\xi$$

where

$$\int_{-\alpha}^{\alpha}s(x,\xi)\sigma_n(x)dx=\lambda_n\sigma_n(\xi)$$

$$\sum_{n=0}^{\infty}\sigma_n(x)\sigma_n(\xi)=\delta(x-\xi) \qquad \text{for } -\alpha<x,\xi<\alpha$$

$$\int_{-\infty}^{\infty}\sigma_n(x)\sigma_m(x)dx=\delta_{nm}$$

and in the frequency domain

$$O(\omega)=\sum_{n=0}^{\infty}a_n\psi_n(\omega)$$

$$a_n=\frac{1}{\lambda_n}\int_{-\Omega}^{\Omega}O(\omega')\psi_n(\omega')d\omega'$$

$$\lambda_n=\frac{1}{\sqrt{\pi}}\Omega\alpha[R_{on}^{(1)}(\Omega\alpha,1)]^2$$

$$\psi_n(\omega)=\sqrt{\lambda_n/N_n}S_{on}(\Omega\alpha,\omega/\Omega)$$

$$N_n=\int_{-1}^{1}(S_{on}(\Omega\alpha,t))^2dt$$

This approach has been used for restoration in diffraction limited imaging systems, with the sinc as the kernel, and also for resolving double stars. In theory, it solves the reconstruction problem for any object whose image is described by a convolution.

Techniques based on the statistical theory of signal prediction have been developed to remedy degradation which consists of both blur and spatially stationary stochastic noise superimposed before and after imaging. The solution of the imaging equation is estimated statistically rather than determined analytically by applying an "optimal" linear filter to the picture. One kind of optimal filter minimizes the mean square error of reconstruction between the restored picture and the undistorted but unknown original [74, 195, 233]; another is a filter which maximizes the signal to noise ratio [46, 154]. One can also seek a Bayesian estimate of the object, i.e., the estimate which maximizes its posterior probability density. The PSF itself may also be considered as stochastic; it may be randomly chosen from a population of PSF's which are independent of the additive noise. Methods such as these are pertinent to restoration of quantum limited images such as isotope scans and images degraded by atmospheric turbulence (also see [226]).

Further discussion of resolving power and restoration will be found in [40, 66, 67, 115, 135, 174, 186, 215].

ENHANCEMENT

Whereas restorative enhancement is the art of making things seem what they are, non-restorative enhancement is the art of making things seem what they aren't. An optimally or even fully restored image may not be the most efficient form for visual data which are to undergo further processing and interpretation by man or machine. Information is returned in an unselective and unorganized way, independent of the semantic content and complexity of the scene. Furthermore, imperfect restoration may leave the image adulterated by residual noise and pseudo-objects—points, curves and even regions. Disorganized or random noise usually takes the form of additions or deletions of signal over relatively small picture areas, with no obvious pattern. Organized noise displays a higher degree of spatial correlation, and takes the form of structured artifacts and systematic biases. Moreover, perceptual artifacts occur because of spatial and tonal quantization; these include artifacts of segmentation and coalescence ("false" contours and "false" regions).

Thus, whether people or machines do the final image processing, non-restorative preprocessing may be a worthwhile and even necessary intermediate step. No enhancement technique, however, can add to the amount of information in the original scene. On the contrary, by selective suppression and accentuation, enhancement re-presents, and information is inevitably lost. It is obviously important to make optimal use of prior information in deciding what to retain.

In general, it is desirable to deemphasize or discard irrelevant material and *at the same time* to emphasize or clarify features and objects of interest. Moreover, it is desirable to do this without having to identify or recognize specific objects, insofar as possible. Deemphasis is usually achieved by using smoothing or integrating operators, but these tend also to blur detail. Emphasis is usually accomplished by sharpening or differentiating operators, or by feature enhancers or contrast enhancers, but these also tend to accentuate noise. However, smoothing *without* obliteration of the relevant and sharpening *without* amplification of the irrelevant are the desired ends. Thus a judicious selection of techniques is required to balance these counter-tendencies and give optimal enhancement.

Enhancement operations can be classified as context-free or context-sensitive. Context-free enhancement consists in repeated and impartial use of a position invariant (and sometimes rotation invariant) procedure, usually determined a priori. Context-sensitive enhancement differs in that decision rules are used to determine the applicability of the various processors and to assign suitable values to processor parameters, in response to local image characteristics. (This is analogous to the use of priority controllers in mechanical languages, for deciding applicability and sequencing of grammatical transformations.) Context-sensitive enhancement is adaptive in the sense that the precise course of processing depends on accumulated experience with the given picture or similar pictures. Although simple, high-contrast or binary material can often be handled using context-free methods, pictures with high information content and noise generally require context-sensitivity.

Enhancement of regions and contours can be described in spatial or spectral terms, but the former predominates. The mathematics of enhancement differs little from the mathematics of restoration, and involves similar difficulties. While restoration deals with entire spectra and means of obtaining well-behaved inverse operators, emphasis and deemphasis deal with parts of spectra. Just as in restoration, there has been much reliance on linear and quasi-linear operators; pictures are convolved with suitable spatial masks, or their spectra are multiplied by frequency filters. Parameters of the masks include mask size, shape, sampling pattern, orientation, and weights. Filter parameters include location in the frequency domain, extent and shape. These parameters remain fixed in context-free enhancement. An important recent development is the advent of contextual processing. Variable-sized neighborhoods as well as non-linear decision logic with changing thresholds are already being used to determine whether to process or not, and how. It will not be surprising to see variable frequency filters used in the near future.

Few of the heuristics introduced in the early literature were justified rigorously; rather, they were based on intuition. Even so, they were usually effective on simple material. As the use of advanced mathematical tools such as spectral analysis, integral transforms, topology and non-parametric statistics became more widespread, systematic procedures for synthesizing processors were developed, and intuitive approaches were either justified or supplanted. However, much remains to be done in improving algorithms and automatically determining applicability and sufficiency criteria.

For purposes of exposition it is convenient to organize the discussion as follows:

(1) spatial smoothing of regions;
(2) spatial smoothing and sharpening of edges;
(3) smoothing and sharpening by spectral manipulation (frequency filtering);
(4) contrast enhancement by manipulation of the gray scale and sampling lattice;
(5) contour enhancement.

Unless otherwise indicated, we assume digitized images, defined by a rectangular sampling lattice and represented by matrix notation.

Smoothing of regions

Most primitive enhancement operations use convolution (spatial masking). Assuming a rectangular sampling lattice, the picture is represented by an M x N matrix

$$P=\{p_{ij} \mid 0\leq i\leq M, 0\leq j\leq N\}$$

The primitive enhancer is a smaller mask consistent with this sampling lattice:

$$W=\{w_{ij} \mid 0\leq |i| \leq m, 0\leq |j| \leq n\}$$

where $m\leq M$, $n\leq N$. The elements of the transformed image T produced by convolving W with P are weighted local averages or finite differences, depending on the algebraic signs of the mask weights:

$$T_{ij}=\sum_{p=-m}^{m}\sum_{q=-n}^{n} w_{pq}\, p_{i+p,\, j+q} \quad (m\leq i\leq M-m,\ n\leq j\leq N-n)$$

No explicit provision has been made here for transforming border elements with subscripts $1\leq i<m$ or $M-m<i\leq M$ and $1\leq j<n$ or $N-n<j\leq N$; this is a serious problem with large masks.

Convolution can be interpreted in various ways. Each mask is dual to a filter in the frequency domain, and conversely, as discussed later in this section. The mask weights may also be thought of in terms of some locally best-fitting surface. Masks corresponding to planar local fits are sometimes called linear, and those corresponding to higher order surfaces are called non-linear. In spite of the low ratio of number of samples to number of estimated coefficients, good quadratic approximations are obtained for even small (3x3) neighborhoods.

The simplest smoothing procedures for regions make direct use of such masks, the number of entries in each direction and their values being fixed. When mask entries are identical, each point of the transformed image is a simple average of original values in its vicinity. When the entries are unequal, the average is weighted. One reason for unequal weights is to adjust for the unequal distances of a non-central mask point from the central point. A more important reason is to allow the weighting patterns to reflect specific noise and correlation characteristics of the image. For smoothing, weights that decrease monotonically from the central position are most commonly used.

In general, the larger the mask size, the more homogeneous the transformed image, but the poorer the rendition of fine detail and significant transitions. It is therefore desirable to introduce optimal procedures in which the decision to smooth or not to smooth and the nature of the smoothing vary from one point of application to another. (This type of variable smoothing is analogous to the use of context sensitive grammatical substitution rules, but the motivation is quasi-statistical rather than syntactical.)

One example of selective smoothing is the removal of isolated bursts of noise on the basis of their characteristic size and light-dark pattern. In binary pictures, the well-known isolated 1's—isolated 0's routines [33, 35, 89, 99, 134, 218, 219] replace a 1(0) if it is completely surrounded by 0's (1's). In binary pictures, for example, holes in the neighborhood of E

$$\begin{array}{ccc} A & B & C \\ D & E & F \\ G & H & I \end{array}$$

can be filled by

$$T(E) = E + AI + BH + CG + DF$$

and isolated points removed by

$$T(E) = E(B+C+F)(D+G+H) + E(D+A+B)(F+I+H)$$

This method is readily extended to grayscale pictures: (a) if the difference between, or the ratio of, a gray value and the local average exceeds a threshold t_1, replace it by the local average; or (b) if the difference or ratio exceeds a threshold t_2, do not smooth [54, 55, 90, 143]. These rules are inconsistent, but the paradox is resolved if it is realized that they are intended for dissimilar material, (b) being appropriate for preserving high contrast detail. They can be combined into a two-threshold rule: (c) smooth if the measure of local heterogeneity is greater than t_1, but less than t_2. The choice of threshold is critical, but criteria have not been formalized. Some of the currently used threshold selection techniques will be discussed later.

Like local averaging, additive or multiplicative superposition of replicas tries to improve the signal to noise ratio by increasing sample size. By replacing the gray value at a point with an arithmetic or geometric mean of several well-aligned copies, substantial reduction in variance is achieved. However, in the multiplicative method, one spurious low value can cancel the reinforcing effect of many high values [90, 100]. Furthermore, in the additive method, low contrast periodic patterns are superimposed on the picture by repeated smoothing [225].

Another approach adjusts neighborhood size in order to improve signal precision. For example, in converting dot patterns to quantized grayscale pictures on the same sampling lattice, the gray value in the transformed image should be proportional to local dot density in the original. A gray value estimate can be based on the reciprocal neighborhood size needed to accumulate some prespecified dot count [160]. Generalizing this to grayscale pictures, a cumulative or integrated gray value for each point can be computed, using a nest of quasi-circular neighborhoods. The reciprocal neighborhood size needed to attain a specified cumulative gray value is used to define the gray value estimate. Criteria for selecting a threshold for the cumulative signal as a function of signal-to-noise ratio are discussed by Pizer and Vetter in this volume. The method, however, deteriorates in regions of high flux or anisotropic distribution of signal.

Biases and errors in the assignment of spatial coordinates to received signals also affect homogeneity of regions and location of boundaries. The method of dot shifting tries to cope with internal smoothing and edge enhancement simultaneously. The principle is to redistribute the gray value at a point toward the a posteriori most probable point of origin. Thus light points near light regions are shifted toward them; similarly for dark points.

The techniques described above aim at making regions appear more homogeneous with respect to local gray values and their variances. This is a special case of the problem of making regions appear more homogeneous with respect to local gray value distributions or to distributions of other surface functions. An example is recent work on texture filling and smoothing discussed in the paper by Rosenfeld and Lipkin in Section III.

Enhancement of edges

Enhancement of edges and their features is one of the oldest goals of analog and digital picture processing. This concern with gray value and curvature gradients has been reinforced by numerous psychophysical and neurophysiological experiments which suggest that boundaries and corners contain a significant proportion of the useful pictorial information [9, 10, 34, 41, 61]. For expository convenience, we distinguish between enhancement of edges and enhancement of contours. In our usage, edge enhancement involves context free algorithms which make no assumptions about continuity, whereas contour enhancement involves algorithms which are concerned with the topology of curves or outlines. Enhancement methods of both types are closely related to edge detection and hence also to picture segmentation or articulation.

Edge enhancement includes those elemental operations which accentuate fluctuations in gray value or any other surface function $p(x,y)$. Unless precautions are taken, however, noise is accentuated when edges are sharpened. We have already discussed restorative enhancement operations. The most effective non-restorative methods use some type of spatial differentiation. The directional derivative of $p(x,y)$ at a point (x_0,y_0) in the direction ξ relative to the x-y coordinate system is defined by a limiting process in that direction,

$$\left.\frac{\partial p}{\partial \xi}\right|_{(x_0,y_0)} = p_x(x_0,y_0)\cos\xi + p_y(x_0,y_0)\sin\xi$$

If the partial derivatives of p in *any* two orthogonal directions are known, then any directional derivative can be computed, provided that p is well-behaved. The gradient $\nabla p(x_0,y_0)$ at that point is a vector parallel to the direction of maximum spatial rate of change and equal in magnitude to that rate. This distinguished direction has direction cosines

$$p_x \Big/ \sqrt{p_x^2+p_y^2} \quad \text{and} \quad p_y \Big/ \sqrt{p_x^2+p_y^2}$$

and the gradient magnitude is

$$|\nabla p(x_0,y_0)| = \left.\sqrt{p_x^2+p_y^2}\right|_{(x_0,y_0)}$$

Other useful combinations of derivatives include the Laplacian operator, a scalar isotropic extension of the second derivative:

$$\nabla^2 p(x_0,y_0) = p_{xx}(x_0,y_0) + p_{yy}(x_0,y_0)$$

and the bi-Laplacian

$$\nabla^4 p = p_{xxxx} + 2p_{xx}p_{yy} + p_{yyyy}$$

The nth order generalized derivative is defined in terms of the partial derivative operators $\partial/\partial x$ and $\partial/\partial y$ as follows:

$$\nabla^n p(x_0,y_0) = \left(\frac{\partial}{\partial x}+\frac{\partial}{\partial y}\right)^n p(x_0,y_0)$$
$$= \sum_{j=0}^{n} \binom{n}{j} \frac{\partial^j}{\partial x^j} p(x_0,y_0) \frac{\partial^{n-j}}{\partial y^{n-j}} p(x_0,y_0)$$

Only even order derivatives with constant coefficients can be combined into isotropic linear operators:

$$T(x,y) = Ap(x,y) + B\nabla^2 p(x,y) + C\nabla^4 p(x,y) + \ldots$$

The simplest of these has been called the crispening or contour enhancement operator [53, 102, 103]

$$T_1(x,y) = Ap(x,y) - \gamma^2 \nabla^2 p(x,y)$$

It can be shown that this operation is the first approximation of a restoration procedure to compensate for blurring caused by a diffusion process or gaussian spread function. A practical optimum is reached by selecting γ^2 as double the steepest gradient appearing in the unenhanced image. The crispening is due to generation of a small but perceptible signal overshoot at the start and end of a slope, an effect reminiscent of the Mach effect [23, 172].

Derivatives of all orders can be used to form isotropic nonlinear differential operators, provided that derivatives of odd order appear only in even functions. The simplest of these

$$T_2(x,y) = A(\nabla p(x,y))^2$$

is the squared gradient.

Various digital masks have been proposed to approximate these differential operators. The appearance of the processed pictures remains surprisingly constant for most of these, although they generate disparate numerical values. However, when spatial differentiation is going to be the basis of quantitative processing, the choice is no longer immaterial.

Computation of gradients involves a nonlinear combination of approximations $\dot{p}_x$ and $\dot{p}_y$ to the partial derivatives in orthogonal directions. Mask weights for the approximations sum to zero. Often $|\dot{p}_x| + |\dot{p}_y|$ is used in preference to the more exact

$$|\nabla p| = (\dot{p}_x^2 + \dot{p}_y^2)^{1/2}$$

The crudest proposal uses 2x2 masks, yielding

$$\dot{p}_x = p_{i,j+1} - p_{ij}$$
$$\dot{p}_y = p_{i+1,j} - p_{ij}$$

The masks can be written symbolically as

$$\begin{array}{rr} -1 & 0 \\ 1 & 0 \end{array} \quad \text{and} \quad \begin{array}{rr} -1 & 1 \\ 0 & 0 \end{array}$$

A more precise estimate is obtained by fitting a quadratic surface over a 3x3 neighborhood by least squares, and then computing the gradient for the fitted surface. The masks are

$$\dot{p}_x: \begin{array}{rrr} 1 & 0 & -1 \\ 1 & 0 & -1 \\ 1 & 0 & -1 \end{array} \quad \text{and} \quad \dot{p}_y: \begin{array}{rrr} 1 & 1 & 1 \\ 0 & 0 & 0 \\ -1 & -1 & -1 \end{array}$$

Fig. 6 has been spatially differentiated in this way, using these masks to approximate the true gradient and displaying the gradient magnitudes as gray values. The gradient direction at each point has direction cosines $(\dot{p}_x/|\nabla p|, \dot{p}_y/|\nabla p|)$.

Information is lost in the preceding computation because the value at the center is not used. Better resolution is obtained by interpolating the image at points midway between nearest neighbors in the sampling lattice, and computing gradients at the inserted points. With a 4x4 neighborhood to fit a quadratic surface with six parameters, the following results are obtained:

sampling lattice

$$\begin{array}{cccc} \cdot & \cdot & \cdot & \cdot \\ \cdot & \cdot & \cdot & \cdot \\ \cdot & \cdot\,* & \cdot & \cdot \\ \cdot & \cdot & \cdot & \cdot \end{array}$$

. sampled points
* interpolated point

interpolated picture

$$\begin{array}{rrrr} -3 & 2 & 2 & -3 \\ 2 & 7 & 7 & 2 \\ 2 & 7 & 7 & 2 \\ -3 & 2 & 2 & -3 \end{array}$$

x-derivative

$$\begin{array}{rrrr} -3 & -3 & -3 & -3 \\ -1 & -1 & -1 & -1 \\ 1 & 1 & 1 & 1 \\ 3 & 3 & 3 & 3 \end{array}$$

y-derivative

$$\begin{array}{rrrr} -3 & -1 & 1 & 3 \\ -3 & -1 & 1 & 3 \\ -3 & -1 & 1 & 3 \\ -3 & -1 & 1 & 3 \end{array}$$

Laplacian

$$\begin{array}{rrrr} 1 & 0 & 0 & 1 \\ 0 & -1 & -1 & 0 \\ 0 & -1 & -1 & 0 \\ 1 & 0 & 0 & 1 \end{array}$$

Gradients can also be found approximately by using a set of oriented edge detectors and searching sequentially at each point for the best match. Gradient magnitude is equated with the maximum response and

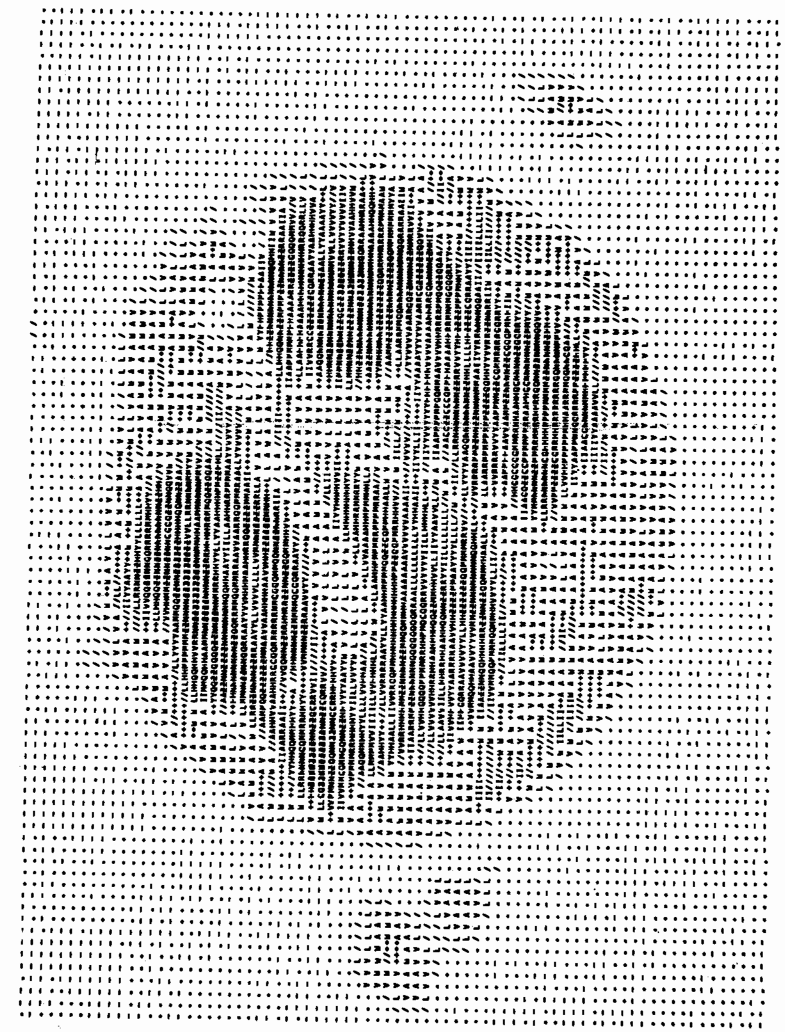

Figure 6a. Spatial differentiation: Image of leukocyte from normal human blood. The cell has been stained and scanned at 800x; the original 256-value grayscale has been compressed to 32 levels.

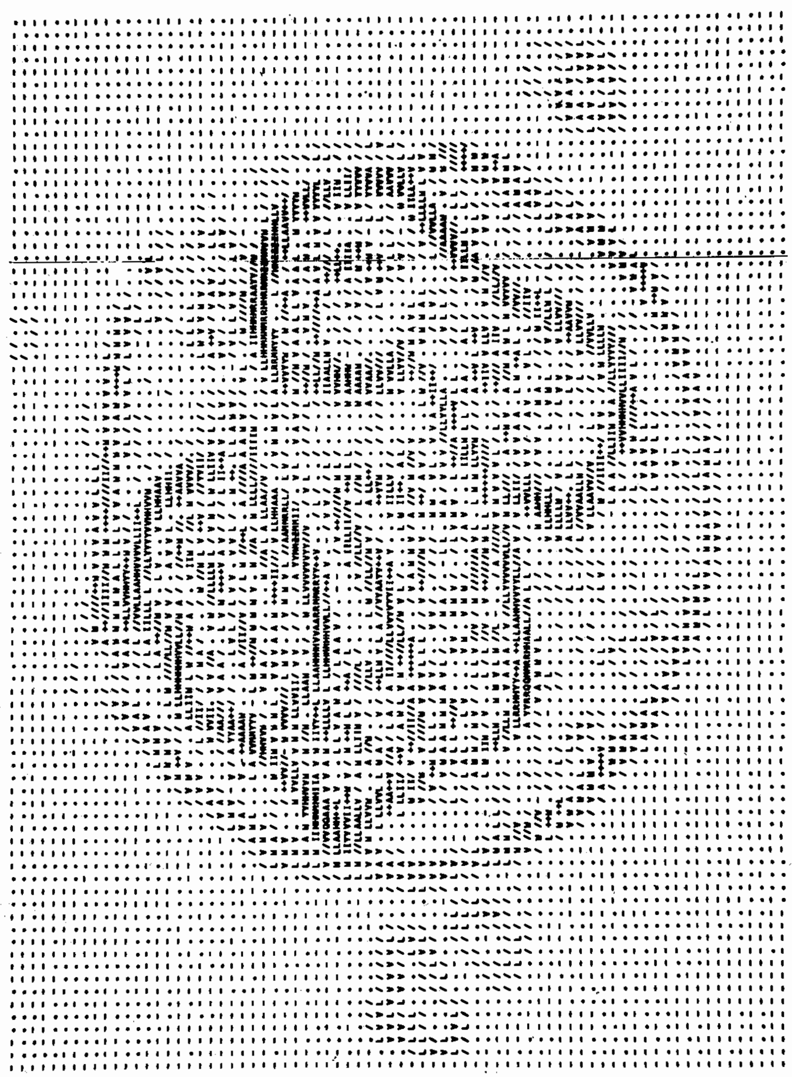

Figure 6b. Differentiated cell image, with gradient magnitudes displayed as a grayscale image. Numerical values correspond to gradients of the best local quadratic fits to the image.

direction is taken parallel to the orientation of the corresponding detector. Such a set is given by the eight masks

$$\begin{matrix} 1 & 1 & 1 \\ 1 & -2 & 1 \\ -1 & -1 & -1 \end{matrix} \qquad \begin{matrix} 1 & 1 & 1 \\ -1 & -2 & 1 \\ -1 & -1 & 1 \end{matrix} \qquad \begin{matrix} -1 & 1 & 1 \\ -1 & -2 & 1 \\ -1 & 1 & 1 \end{matrix} \qquad \begin{matrix} -1 & -1 & 1 \\ -1 & -2 & 1 \\ 1 & 1 & 1 \end{matrix}$$

$$\begin{matrix} -1 & -1 & -1 \\ 1 & -2 & 1 \\ 1 & 1 & 1 \end{matrix} \qquad \begin{matrix} 1 & -1 & -1 \\ 1 & -2 & -1 \\ 1 & 1 & 1 \end{matrix} \qquad \begin{matrix} 1 & 1 & -1 \\ 1 & -2 & -1 \\ 1 & 1 & -1 \end{matrix} \qquad \begin{matrix} 1 & 1 & 1 \\ 1 & -2 & -1 \\ 1 & -1 & -1 \end{matrix}$$

Fig. 7a was obtained by applying this algorithm to a 256-level image of a white blood cell. Gradient values below 11 were suppressed for clarity. In Fig. 7b, the symbols –, L, /, and I were used to encode isopleth directions at points with above threshold gradients.

For digital Laplacians, both cross and square shaped neighborhoods have been used, the weights also always summing to zero. Only simple convolution with the picture is needed. Examples are

$$\begin{matrix} 0 & -1 & 0 \\ -1 & 4 & -1 \\ 0 & -1 & 0 \end{matrix} \qquad \begin{matrix} -1 & -1 & -1 \\ -1 & 8 & -1 \\ -1 & -1 & -1 \end{matrix}$$

(See [11] for a discussion on masks, and see [6] for a discussion of analog sharpening methods.)

The main weakness of the preceding techniques is their treatment of signal and noise, resulting in overemphasis of accidental fluctuations. This can be controlled in two ways [50]. First, contour enhancement without noise enhancement can be realized by replacing the Laplacian in the crispening operator with the second derivative in the direction n of the local gradient. The modified transformation is

$$T_2(x,y) = p(x,y) - \gamma^2 \frac{\partial^2 p}{\partial n^2}$$

$$\frac{\partial^2 p}{\partial n^2} = \frac{\dfrac{\partial^2 p}{\partial x^2}\left(\dfrac{\partial p}{\partial x}\right)^2 + 2\dfrac{\partial^2 p}{\partial x \partial y}\dfrac{\partial p}{\partial x}\dfrac{\partial p}{\partial y} + \dfrac{\partial^2 p}{\partial y^2}\left(\dfrac{\partial p}{\partial y}\right)^2}{\left(\dfrac{\partial p}{\partial x}\right)^2 + \left(\dfrac{\partial p}{\partial y}\right)^2}$$

Second, contour enhancement along the gradient and smoothing along the contour can be realized by replacing the Laplacian with a mixture of second derivatives normal (direction n) and tangential (direction t) to the contour:

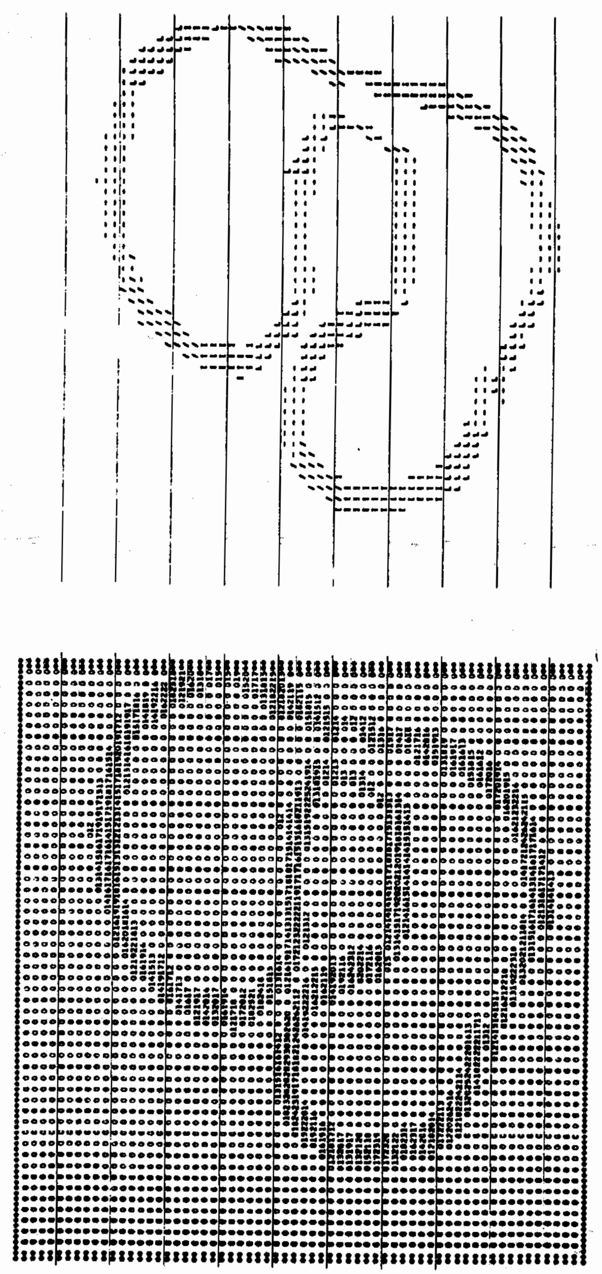

(a) (b)

Figure 7. Spatial differentiation. The result of applying eight 3 x 3 oriented edge detectors to a leukocyte image. Only the nucleus of this white blood cell is seen. (a) Each two-digit value indicates the maximum figure of merit for the eight detectors at the corresponding image point, provided this value exceeds a threshold selected to de-emphasize noise. (b) Orientations of the maximally correlating edge detectors, quantized to four directions, N-S, E-W, NE-SW, and NW-SE, which are denoted by the symbols —,l,/, and L.

$$T_3 = p - \lambda^2\left(\frac{\partial^2 p}{\partial n^2} - \frac{1}{3}\frac{\partial^2 p}{\partial t^2}\right)$$

$$\frac{\partial^2 p}{\partial t^2} = \frac{p_{xx}p_y^2 - 2p_{xy}p_x p_y + p_{yy}p_x^2}{p_x^2 + p_y^2}$$

At least nine-point interpolation is needed. Using a 3 x 3 square neighborhood of half-width d or an octagonal neighborhood of radius d

$$\begin{matrix} p_{-1-1} & p_{-10} & p_{-11} \\ p_{0-1} & p_{00} & p_{01} \\ p_{1-1} & p_{10} & p_{11} \end{matrix}$$

$$p_x = (p_{10} - p_{-10})/2d$$
$$p_y = (p_{01} - p_{0-1})/2d$$
$$p_{xx} = (p_{10} + p_{-10} - 2p_{00})/2d^2$$
$$p_{xy} = (p_{11} + p_{-1-1} - p_{-11} - p_{1-1})/4d^2$$
$$p_{yy} = (p_{01} + p_{0-1} - 2p_{00})/2d^2$$

Similarly, lines and edges can be emphasized in selected directions and at the same time suppressed in others. Edge enhancers are masks partitioned by a line of like slope, with entries of opposite sign on opposite sides of the divide. The line enhancer consists of a like oriented ridge of 1's on a field of −1's. A typical set of 7 x 7 masks which can be used for line enhancement, and as we shall see, for detection also, is [42, 73, 137, 145]:

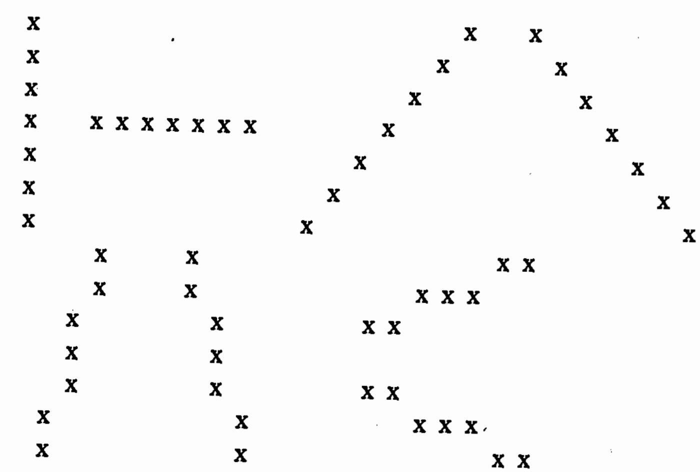

Features and shapes can be enhanced similarly, although several templates of different scale may be needed in order to span the size range. For example, corner, intersection and spot enhancers would take the following general forms:

```
– – – –
– – – –
– – + +
– – + +
```

```
      – + –
      – + –
– – – + – – –
+ + + + + + +
– – – + – – –
      – + –
      – + –
```

```
        – – –
      – – – – –
    – – + + + – –
  – – + + + + + – –
  – – + + + + + – –
  – – + + + + + – –
    – – + + + – –
      – – – – –
        – – –
```

These enhancers are closely related to the optimum templates for certain patterns (see the next section).

Frequency filtering

Two-dimensional spectral analysis is the only systematic approach now available for describing the effects of spatial masks in terms of resolution and noise. Since the system MTF and PTF describe the rendition of detail, masks can be classified according to the action of the corresponding frequency filters. A qualitative classification into (1) low pass, (2) high pass, (3) low emphasis, (4) high emphasis, and (5) band pass filters is convenient. Masks should be symmetric about the central element if isotropy is desired, and asymmetric if directional information is to be emphasized. Most imaging systems preserve low frequencies well but respond increasingly poorly to high frequencies (Fig. 8a); thus, global information is usually preserved intact, but detail is compromised.

The main function of the low pass filter (Fig. 8b) is to retain low frequency information and reject high frequencies. Thus, low pass filtering is related to smoothing attributable to random noise. The challenge is to select a cutoff frequency ω_0 so that the filter is narrow enough to remove noise, but wide enough to preserve detail; or, in the spatial domain, to select a mask smaller than the smallest detail to be retained.

The purpose of the high pass filter is to remove low frequencies corresponding to background and to enhance contrast. Thus, high pass

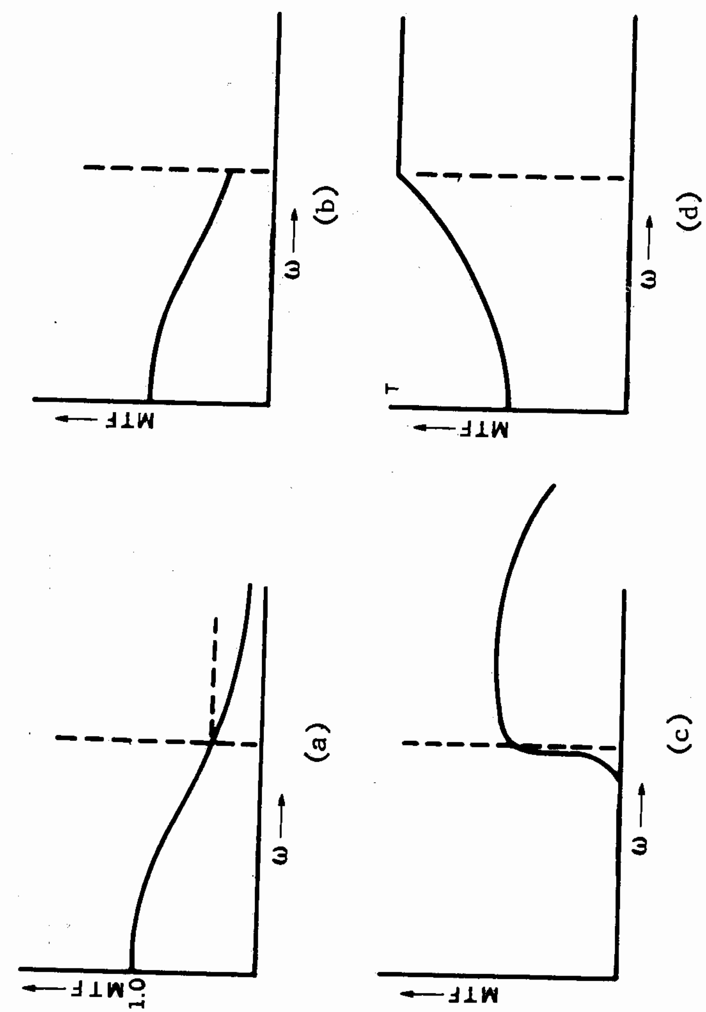

Figure 8. Principles of frequency filtering: (a) a typical system MTF with cut-off frequency separating relevant from irrelevant detail; (b) low pass filter; (c) high pass filter; (d) high emphasis filter. After Nathan [143].

filtering is related to sharpening. A spatial mask used for this purpose must be larger than the largest differential feature to be retained.

If $V=\{v_{kl}\leq 1 \mid 0\leq |k| \leq K, 0\leq |l| \leq L\}$ is a low pass mark, then $W=\{w_{kl} \mid w_{kl}=\delta(k)\delta(l)-v_{kl}, 0\leq |k| \leq K, 0\leq |l| \leq L\}$ is a high-pass filter.

A band pass filter retains frequencies between two limits and is equivalent to a low pass, high pass pair.

High and low emphasis filters try to compensate for spectral losses and to stretch contrast, but not at the risk of disregarding useful information. The simplest low emphasis mask is an equal weight mask. Emphasis of high frequencies can be achieved by superimposing a scaled high pass transform τ on the original image p:

$$t_{ij}=p_{ij}+\epsilon\tau_{ij}$$

where ϵ is adjusted according to some external criterion. The Laplacian mask can be regarded as a scaled equal weight mask superimposed on the original image; the result is a high emphasis transform.

It is straightforward to determine the effect of a given mask on the frequency spectrum. The image sampled at interval d

$$p(x,y)=\sum_{n=-\infty}^{\infty}\sum_{m=-\infty}^{\infty} i(md,nd)\,\delta(x-md)\,\delta(y-nd)$$

has a Fourier series for its Fourier transform:

$$\overline{P}(u,v)=\sum_{n=-\infty}^{\infty}\sum_{m=-\infty}^{\infty} i_{mn}e^{-2\pi i(um+vn)d}$$

The Fourier transform of the sampled convolved image

$$t(m,n)=\sum_{k,l}\omega_{kl}p_{m-k,\,n-l} \qquad (m,n=0,\pm1,\ldots)$$

satisfies a convolution-product theorem

$$\overline{T}(m,n)=\overline{W}(m,n)\overline{P}(m,n)$$

where the mask transform

$$\overline{W}(m,n)=\sum_{k=-K}^{K}\sum_{l=-L}^{L}\omega_{kl}e^{-2\pi i(mk+nl)d}$$

completely characterizes the processing. For example, the equal weight mask corresponds to a low pass filter, since its transform consists of equal amplitude sinusoids which tend to interfere; the larger the mask, the more restrictive the filter.

The problem of finding a mask corresponding to a specified frequency filter is more difficult. If the filter is band pass (zero outside a finite frequency range), then the exact mask for $\overline{W}(u,v)$,

$$\omega_{kl}=\overline{W}(u,v)e^{2\pi i(uk+vl)}dudv$$

is infinite and unrealizable, so a finite approximation $\{\dot{\omega}_{kl}\}$ which is optimal in some sense is desired. Possible figures of merit which measure the closeness of fit of $\overline{W}$ and $\dot{W}$ are minimal integrated mean square error and minimal maximum absolute error, both over the frequency domain [7, 8, 14, 15, 30, 38, 47, 91, 111, 113, 147, 151, 193, 216, 221, 234].

Manipulations of the gray scale and the sampling lattice

Selective contrast enhancement and prevention of false contours can often be obtained by direct manipulation of the gray scale, or by spatial and grayscale requantization. Most quantization schemes involve a fixed number of gray levels which are apportioned uniformly over the dynamic range of the system. In addition to the possibilities of creating spurious contours and obscuring genuine ones, this method of recording information is wasteful in an information theoretic sense. If the grayscale statistics of input images can be determined, it is possible to quantize optimally [87, 188, 235] by reconcentrating the levels in the most informative part of the scale. Failing in this, refinement of the scale (increased number of gray levels) may be necessary.

A similar distortion of the gray scale is effected by the type of contrast enhancement referred to as gamma correction. Although gamma correction originally referred to gray scale and contrast adjustments intended to compensate for uneven or nonlinear responses of the image sensor, the term can be generalized to include any continuous transformation of the gray scale. The selected function differentially stretches portions of the gray scale and compresses others; signals are suppressed in low-slope portions of the curve and expanded in high-slope portions. The function of Fig. 9a clips extreme dark and light values and enhances the renditions of the gray values. A variant of this uses continuous functions as in Fig 9b. The same set of gray values is used to

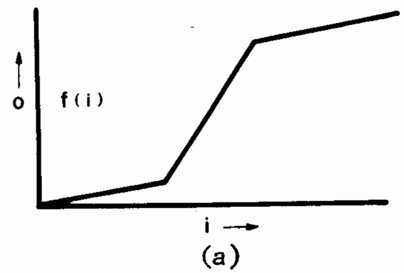

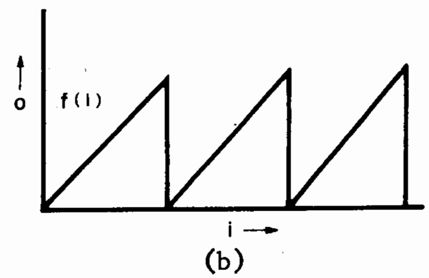

Figure 9. Contrast enhancement by functional transformation of the gray scale. Output gray value is shown as a function of input gray value: (a) gamma correction; (b) level slicing.

represent several different ranges of input levels, in the hope that continuity and context will eliminate ambiguity. In the often eye catching results, everything in the image is shown at high contrast, but the creation of false contours, corresponding to discontinuities of f, may be seriously misleading [124, 159, 161].

Paradoxically, the appearance of a grayscale picture can be improved by introducing random noise. Presumably, this added noise is sufficient to disorganize irrelevant fine detail, undesirable (false) contours and regions, and overly stylized boundaries, but is insufficient to disturb major patterns. The simplest method incorporates random additive noise of known distribution at each point [88, 175]. A more complicated approach uses random walk noise. Each image point is exchanged with another at a distance selected according to a known probability distribution, but in a randomly chosen direction [230].

Finally, bizarre effects may be generated in reconstructing images from digital samples because of the phenomenon of aliasing [155, 162, 167].

Conversion of the continuous image to discrete samples at the rate T non-linearly changes the presampled imaging system MTF(ω) to an infinite series $\sum_{n=-\infty}^{\infty}$ MTF($\omega - n/T$) in a way that may lead to ambiguity in reconstruction if the original MTF(ω) has components of frequency greater than 2/T. The only remedy is readjustment of the sampling interval.

Enhancement of contours and curves

After edge enhancement, contour information is usually extracted. Connected regions can be assigned continuous connected borders which are tracked and encoded; borders require no thinning or gap filling but it may be desirable to smooth them by removing points which cause unnecessary perturbations or sharp variations in curvature.

The following tracking algorithm, which allows horizontal, vertical, and diagonal tracks, will always extract the connected outline of a connected component. Given a labeled connected component, s, an interior point is a point of s which has only points of s in its 3 x 3 square neighborhood; a boundary point is any point of s which has points of s and of the complement of s in its 3 x 3 square neighborhood. The leftmost, uppermost boundary point of s is taken as the outline initium and the current position; its left neighbor is the current antecedent. The remaining points in the 3 x 3 neighborhood are inspected in counterclockwise order, beginning with the antecedent, until another point of the set s called the consequent is found. The local boundary direction is the angle (a multiple of 45°) formed by antecedent, current point and consequent. The current point becomes the antecedent, and the consequent becomes the current point. The search is iterated until the algorithm returns to the initium and the next iteration would lead to a recycle [165].

Although outlines derived in this way are thin, curvature minimizing methods may enhance their appearance. If the contour is chain-encoded [43, 44, and the paper by Freeman in Section II], a set of mechanical reduction rules can be specified [206, 210] for eliminating wasteful or devious paths and reducing curvature. Sometimes these outlines still appear coarse. Smoothness may be enhanced further by constructing a representation in terms of piecewise continuous curvilinear arcs on a new, interpolated sampling lattice. For example, a polygonal contour of minimal length can be fitted to a closed contour by using dynamic programming [52] or non-linear programming [131, 132]. Fourier series can be used to analyze and synthesize contours; a contour can be smoothed by low pass frequency filtering.

Elongated forms or thick contours are usually extracted by clipping or thresholding the original picture or transformations of it. Contours can also be extracted using derivatives, as illustrated in Fig. 6. The resultant contours in either case are often discontinuous, thick, or jagged. The problem is to enhance them—to provide good continuation and closure by filling gaps and eliminating perturbations, and by thinning.

Thinning is the generic name for processes designed to reduce connected elongated objects to line-like representations which preserve connectivity. Many algorithms based on an exfoliative or stripping method have been suggested [89, 99, 114, 126, 140, 187]. The common procedure involves removing boundary points layer by layer, provided that their removal does not erode away ends of arcs and does not destroy connectivity, until the configuration stabilizes. The procedure is noise sensitive in binary pictures and depends critically on the method used to generate the original thick contour. This difficulty can be remedied to some degree by using skeletonization procedures [18, 21, 156, 158] for multi-level pictures which avoid the use of binary intermediates. In this connection, preprocessing with the gray-weighted distance transform [185, 187] gives additional smoothing.

Ensuring that outlines have good continuation clearly requires decision rules utilizing context and feedback. Filling of holes (removing "salt" noise) and removing spurious connections (removing "pepper" noise) are both necessary. Look-ahead procedures predict a position for the next outline point, and trigger a local search; the predicted position is an extrapolation based on assumptions or acquired information about local slope and curvature [62, 79, 85, 104, 169, 229, 231]. Sequential tracking and smoothing can be combined for filling gaps, and separating accidental joins as well. Let $(x_R(k),\ y_R(k))$, $(x_S(k),\ y_S(k))$, and $(x_T(k),\ y_T(k))$ represent the coordinates of the kth sample on the unprocessed, smoothed and thinned tracks, respectively. A smoothed track can be obtained [58] by setting

$$x_S(k)=\frac{3}{4}x_S(k-1)+\frac{1}{4}x_R(k)$$
$$y_S(k)=\frac{3}{4}y_S(k-1)+\frac{1}{4}y_R(k)$$

and the lth point on the thinned track by

$$x_T(l)=x_S(k) \qquad \text{if } |x_S(k)-x_T(l-1)| \geq \text{some } \theta$$
and similarly for y.

A variant [112] uses

$$\begin{aligned} x_S(k) &= x_R(k)-\theta && \text{if } x_S(k-1)<x_R(k)-\theta \\ &= x_R(k)+\theta && \text{if } x_S(k-1)>x_R(k)+\theta \\ &= x_S(k-1) && \text{if } |x_S(k-1)-x_R(k)| \leq \theta \end{aligned}$$

Spurs can be removed by using digital "calipers" to detect and track sharp bends simultaneously [137]. The caliper tips move around the outer boundary in such a way that the arc length between them remains constant. A sharp decrease in the chord length indicates the presence of a spur.

Outlines can also be obtained from thick connected contours by tracking. A digital "probe" is laid across the thick line, and the midpoint of the intersection is determined. As the procedure is repeated at different positions along the line, the midline track is generated [105]. The procedure as reported in the literature is limited to horizontal and vertical probes. If gradients are computed at the boundary, however, orthogonal probes can be generated; but a probe orthogonal to one edge may not be orthogonal to the opposite edge.

OBJECT EXTRACTION

To borrow a term recently introduced in systems theory [236], a pictorial object is a fuzzy set which is specified by some membership function defined on all picture points. From this point of view, each image point participates in many memberships. Some of this uncertainty is due to degradation, but some of it is inherent. The role of object extraction in machine processing, like the role of figure/ground discrimination in visual perception, is uncertainty-reducing and organizational. In fuzzy set terminology, making figure/ground distinctions is equivalent to transforming from membership functions to characteristic functions.

We distinguish two types of processing that are commonly subsumed under the single heading of object extraction: detection and articulation.

Detection is concerned with making decisions about the presence or absence of specific object signals and estimating their position in the field of view. Detection in this sense involves finding optimum matches among a finite set of possibilities. Articulation is concerned with a more detailed structural analysis, in which the picture is punctuated by object delimiters or boundaries, much akin to the insertion of phrase markers in grammatical analysis of sentences. Potential objects, not prespecified, are sought. The parsing defines the final objects and their relationships.

For solving some image processing problems, it may be possible to combine detection and articulation in a multilevel extraction scheme. The detection algorithms would function as coarse scanners, locating potential areas of interest, and the articulation algorithms would function as fine scanners, delineating objects and preparing them for later analysis.

Detection

Detection refers to procedures for locating objects which are prespecified in terms of either a local spatial distribution of gray values (local shape or template) or a transform of such a distribution (filter). The templates or filters can be selected intuitively [168], by self-design [82, 180, 181], by random generation and systematic evaluation [16, 217], by adaptive learning [17, 24, 78, 96, 97, 110, 178] from sets of training images, or by deliberate design according to the principles of statistical communication theory [107, 125, 133, 179]. Spatial correlation, optimum frequency filtering, and other transformations such as moment and orthogonal expansions are the main mathematical tools for object detection.

In a typical application, a picture or some transform is first compared with a library of standardized or representative features and objects or their appropriate transforms. For each possible feature, a figure of merit is computed at each picture point, yielding in effect a new picture transformation which indicates degree of match for that feature throughout the original picture. Using some criterion of significance, each of these transformations can be thresholded and converted to a binary map locating particular instances of the features in the picture. In addition, the various figures of merit at each picture point can be rank ordered.

Cross correlation has been used as a figure of merit almost exclusively. The normalized cross correlation or correlogram of a pattern or template f (figure) with a picture g (ground) is the fraction

$$C(f,g)(x,y)=\frac{\int\int f(u,v)g(u+x,v+y)dudv}{\sqrt{\int\int f^2dudv\int\int g^2dudv}}$$

which is 1 only when the picture is a scaled translation of the pattern: $g=cT_{uv}f$. The correlogram values are high near positions of close match and are sharply attenuated elsewhere, the peak height being a measure of degree of match. However, numerical results are sensitive to changes in orientation, magnification, mean gray value and contrast. At the expense of making the correlogram multidimensional and unwieldy, invariance to changes in these factors can be introduced if desired. It is possible to eliminate gray value and contrast sensitivity by dealing with derivatives (see [117] for a generalization).

It is sometimes useful to detect significant change rather than significant match, without locating the site of this change. The mean absolute and mean squared differences of two pictures have been used as overall or gross measures of disparity [32, 63, 173]. Random generation of templates and filters which are subjected to subsequent evaluation has been attempted for binary pictures. While the same idea might be extended to grayscale pictures, the combinatorics involved and other intrinsic limitations make this approach unattractive.

Learning machines have perhaps been the most widely used methods of template construction [144, 189]. Template weights are adjusted as a sequence of typical features and their identifications are presented, until convergence or stability of the weights is observed. Alternatively, all the information in a sample of representative objects is used to determine optimum weights in one step. These methods do not directly take into account spatial correlations in the pattern, but templates invariably look like the objects they are supposed to represent. Although these approaches have been very successful in character recognition and other high contrast cases, they give little understanding of image structure.

More systematic methods of construction use optimality principles from statistical communication theory. The image is regarded as pattern o plus pattern-independent noise n with a known statistical structure:

$$i(x,y)=o(x,y)+n(x,y)$$

and a filter for the pattern is sought. The filter specifications depend on the cross correlation of signal (i.e., pattern) with noise, and the autocorrelations of signal and of noise. A common type of optimal filter is based on minimizing mean square differences.

More widely used for picture processing is the matched filter, which maximizes the signal to noise ratio. The classical matched filter response maximizes signal energy to noise energy; it detects and locates all translates of the pattern. If $O^*(u,v)$ denotes the conjugate Fourier transform of the pattern $o(x,y)$ and $N(u,v)$ denotes the power spectrum of the noise, then the matched filter F is given by

$$F(u,v)=O^*(u,v)/N(u,v)$$

This concept can be generalized to gradient-matched filters which detect on the basis of edges [4]. Such a filter of order p maximizes energy in the pth order signal gradient to energy in the pth order noise gradient:

$$F_p(u,v)=(-1)^p\frac{(u^2+v^2)^p O^*(u,v)}{N_p(u,v)}$$

where $N_p(u,v)$ is the power spectrum of the pth gradient of the noise. The generalized matched filters of the three lowest orders correspond to three of the filters discussed in the previous section: $p=0$ to an energy filter (a low pass filter); $p=1$ to the gradient, and $p=2$ to the Laplacian (high pass filters). Generalized filters give stronger matches than ordinary matched filters when edges rather than energy describe the signal.

The spatial output of the filter is

$$C_p(x,y)=(\nabla^p o(-x,-y))**(\nabla^p i(x,y))**(R_{N_p}(\tau,T))^{-1}$$

where $R_{N_p}(\tau,T)$ is the autocorrelation function of the pth order noise gradient and ∇^p is the pth order gradient operator. The weights of the corresponding mask resemble the object or object outline to be detected. At exact registration, the filter output in the absence of noise is

$$C_p(0,0)=\iint(-1)^p|O(u,v)|^2(u^2+v^2)^p du dv$$

and in the presence of noise it is

$$C_{p_N}(0,0)=\iint(-1)^p\frac{(u^2+v^2)^p O^*(u,v)}{N_p(u,v)}I(u,v)du dv$$

The correlation parameter $C_{p_N}(0,0)/C_p(0,0)$ thus measures the efficiency of the match procedure.

The optimal spatial mask for a feature can be shown to be dependent on not only its spatial pattern, but also on its internal spatial correlations [5, 213]. This is true irrespective of the noise structure. For example, consider a stochastic mxn digital pattern with expected value $P=(p_{ij})$ and with covariance matrix Σ which consists of an mxm array of nxn matrices Σ_{ij}, where Σ_{ij} is the cross correlation matrix of the ith and jth rows of P:

$$\Sigma_{ij}=E(P_{i\_\_}-E(P_{i\_\_}))(P_{j\_\_}-E(P_{j\_\_}))^T$$

The energy signal to noise ratio for a template $W=(w_{ij})$ is

$$(S/N)^2=(E(C(0,0)))^2/\mathrm{var}(C(u,v))$$

where $C(u,v)$ is the discrete convolution

$$W**P(u,v)=\Sigma_i\Sigma_j w_{ij}p_{i+u,j+v}$$

$E(C(0,0))$ denotes its expected value at perfect registration of W and P, and $\mathrm{var}(C(u,v))$ is the variance of the cross correlation when the template is shifted over the pattern. Since $E(C(0,0))=(W**P)(0,0)$ and $\mathrm{var}(C(u,v))=P^T\Sigma P$, the discrete optimal mask is $F=\Sigma^{-1}P$.

Thus the optimal mask F for a random or uncorrelated pattern is the pattern itself, but for any nontrivial covariance structure, clearly it is not. For instance, if the correlation along a row tapers with distance according to the following autocorrelation matrix

$$\Sigma_{ii}=(\rho^{|r-s|}) \qquad r,s=1,n$$

and if the cross correlation of the ith and jth row tapers according to

$$\Sigma_{ij}=\rho^{|i-j|}\Sigma_{ii}$$

then the optimal mask is

$$\begin{bmatrix} \begin{matrix}\rho^2\\-\rho(1+\rho^2)\\\rho^2\end{matrix} & \begin{matrix}-\rho(1+\rho^2)\\(1+\rho^2)^2\\-\rho(1+\rho^2)\end{matrix} & \begin{matrix}\rho^2\\-\rho(1+\rho^2)\\\rho^2\end{matrix}\end{bmatrix} **P$$

For a random pattern, this becomes the pattern itself; for a maximally correlated pattern, it becomes

$$\begin{bmatrix} 1 & -2 & 1 \\ -2 & 4 & -2 \\ 1 & -2 & 1 \end{bmatrix} **P$$

and the mask approximates a bi-Laplacian type of operator $\partial^4/\partial x^2 \partial y^2$. The general isotropic operator $\Sigma_k \gamma_k \nabla^{2k}$ for this case has as first approximation

$$\begin{bmatrix} 0 & -\rho/2 & 0 \\ -\rho/2 & 1+\rho^2 & -\rho/2 \\ 0 & -\rho/2 & 0 \end{bmatrix} **P$$

This becomes the identity operator for the random scene, and the Laplacian

$$\begin{bmatrix} 0 & -1/2 & 0 \\ -1/2 & 2 & -1/2 \\ 0 & -1/2 & 0 \end{bmatrix} **P$$

for the maximally correlated scene.

The relationship of uncertainty considerations to construction of optimum spatial filters is discussed in [146]. Particularly noteworthy is the development of local shape or feature detectors in [19, 22, 25, 26, 42, 66, 69, 70, 71, 72, 73, 77, 84, 137, 138, 145, 190, 192, 207, 220, 224].

Along similar lines, various mathematical transformations and expansions have been used in the dual roles of detectors and descriptors for simple geometric shapes. These have included moment transforms [1, 20, 86]

$$m_{ij} = \int\int x^i y^j P(x,y)\,dxdy$$

Chebyshev transforms [198] and Haar-Walsh orthonormal representations [51, 60, 118, 227], as well as the previously discussed Fourier transforms [80, 92]. Conceivably, bilinear and other complex conformal transformations may also be useful.

Articulation

In a broad sense, articulation is concerned with the optimal assignment of boundaries to objects. The nontriviality of this task is apparent from careful inspection of multilevel digitizations (see Fig. 10) and

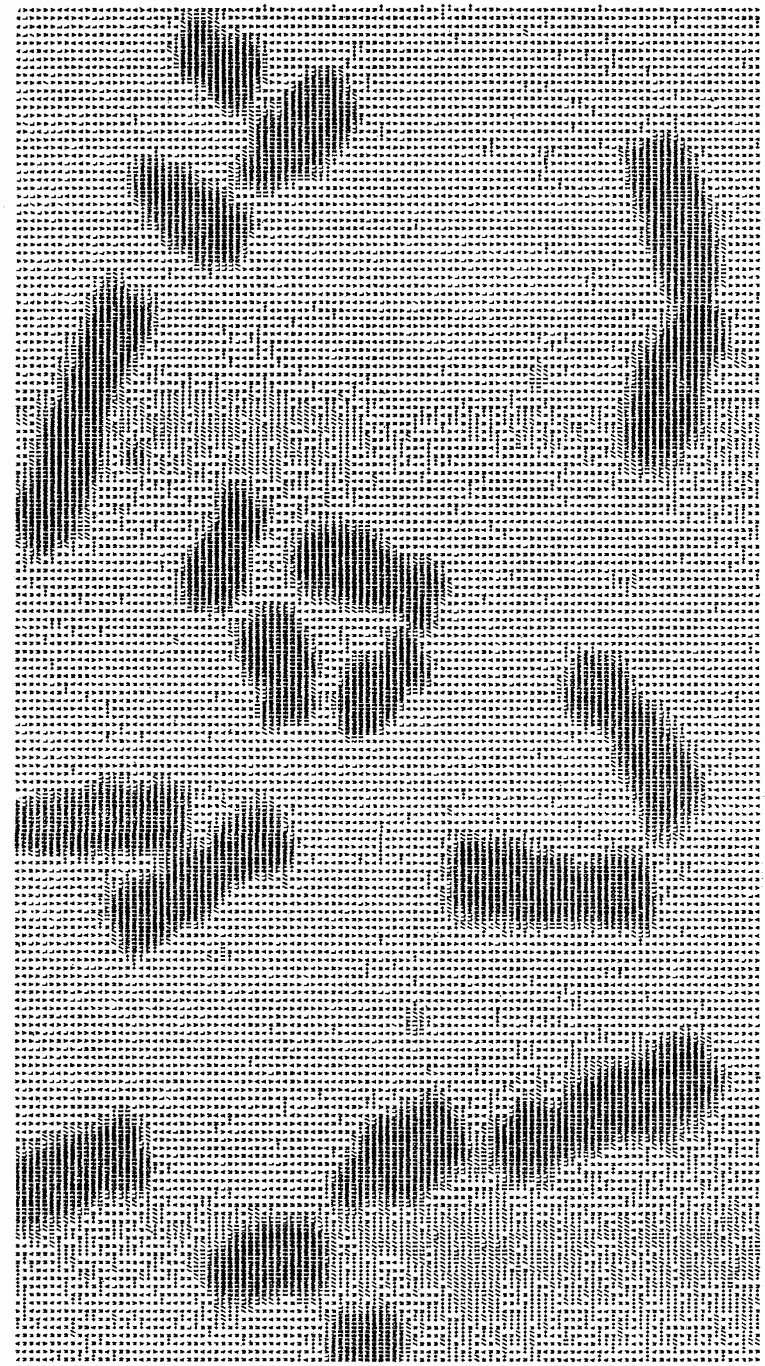

Figure 10. High-magnification, high-resolution image of human chromosomes made with the CYDAC scanner [119]. Although some blur at the edges is inherent in the chromosomes, coalescence of image parts is an artifact due to the transfer characteristics of the imaging system.

"sloppy" binary pictures. There is no generally accepted criterion for assigning a "best" edge location. In grayscale pictures, traces or profiles of "true" edges can have a variety of shapes, depending on the spread functions involved (see Fig. 3). The position of the maximum gradient, which is usually, but not necessarily, found near the center of the edge trace, is the most attractive candidate for defining a unique edge location, but neither it nor the average gradient value over the trace determines how sharp the edge appears to an observer [41, 76, 232]. After restoration or enhancement, however, it would be expected that the maximal gradient should correlate better with the sensation of sharpness. In binary pictures, the issue is rather different: how best to segment a pattern of dots.

Some authors have grouped boundary assignment techniques into parallel vs. sequential. This categorization may not be as illuminating as the observation that some algorithms incorporate a good continuation or closure principle and others do not. Since the fundamental problem is to find connected regions of consistent flux which separate connected regions of constancy, relative to some surface function, a classification into homogeneity-emphasizing and heterogeneity-emphasizing techniques would seem to be more appropriate. Methods of the first type utilize the most redundant parts of the image, while methods of the second type utilize the most informative parts. But even this distinction is more a reflection on historical development than on underlying principles.

Thresholding is the oldest and most widely used method of extraction. It has been used on pictures $p(x,y)$ and on picture transformations $T[p]$. In its most general form, thresholding is a quantization-coarsening transformation T of the form

$$\text{if } t_1 \leq T(p(x,y)) \leq t_2, \text{ then } T(x,y) = c_{12}; \text{ otherwise } T(x,y) = 0$$

where t_1 and t_2 are fixed constants. When thresholding is applied to the picture itself, the presumption is that regions of interest display different, fairly constant gray values. When thresholding is applied to a spatially differentiated picture, e.g., as a clipping operation ($t_2 = \infty$), contouring occurs; i.e., the continuous image is replaced by a series of outlines or cartoons. Although thresholding is very effective on many types of pictorial material, it has noteworthy shortcomings: (1) smoothing and false contouring are byproducts; (2) there is no

guarantee that the resultant contours are connected or closed; and (3) the results are very sensitive to selection of thresholds [119, 142].

Early use of thresholding involved human judgment. However, for moderate to high contrast pictures, machine determination can be based on inspection of a histogram of gray values. One semi-automatic solution used the gray value corresponding to the upper p-tile of the histogram as threshold, where p is externally supplied [36]. Since suitable thresholds differ from picture to picture and even within the same picture, the procedure is of limited value.

By taking advantage of the multimodal nature of the gray value histogram, it is often possible to select thresholds automatically [164]. The method is suitable for pictures in which objects appear on a fairly uniform ground, and objects occupy a greater proportion of image area than edges. Background and objects will generate histogram modes, and edges, comprising a range of intermediate gray values over a smaller area, correspond to antimodes. Fig. 11 shows a histogram for a 256-level image of a white blood cell, the machine selection of two thresholds, and the partitioning into background, nucleus, and cytoplasm that resulted.

This method has been generalized [184] to make use of the second order probabilities that given gray levels occur as neighbors of other gray levels. Clusters of gray levels that have similar sets of neighbors are detected, and thresholds are selected at the boundaries of these clusters.

It is possible to readjust a tentative threshold until the isophote which best coincides with the average maximal gradient is found. In Fig 12a, the mean gray value and mean gradient are plotted as functions of distance inward and outward from a postulated object boundary. Signed distances were determined by a bilateral extension of the distance transform, positive distances being propagated inside the boundary and negative distances being propagated outside the boundary. Fig. 12b gives a gray scale rendition of the results of the distance algorithm. If the postulated boundary corresponds to the actual boundary, the plotted gradient values should peak at distance 0 (the line spread function is the derivative of the edge spread function).

Differentiation, statistical differencing, and image subtraction are heterogeneity-seeking methods. Image subtraction refers to the com-

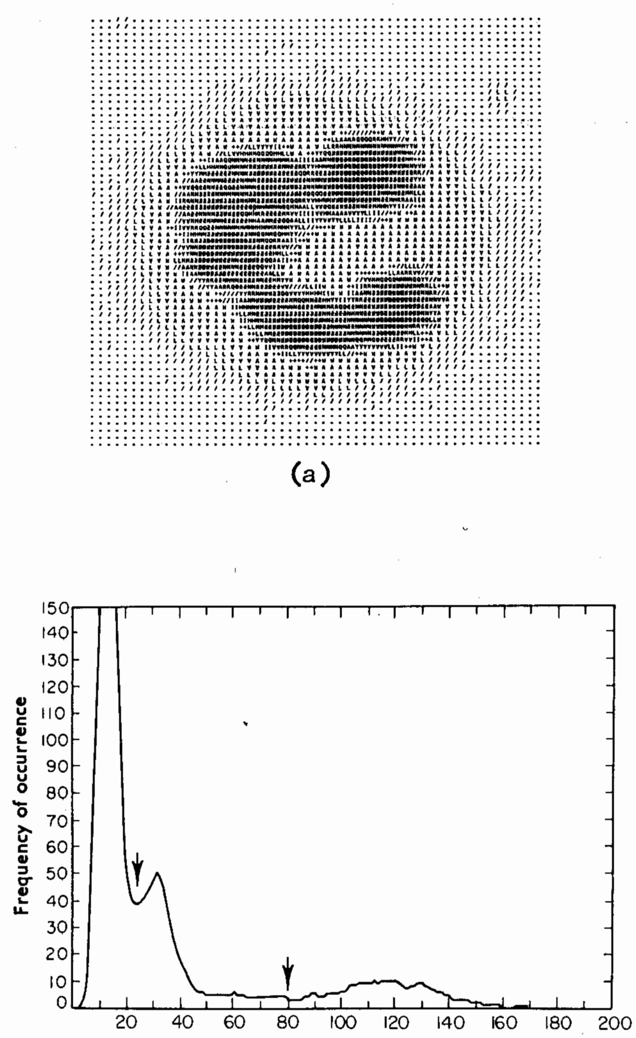

(a)

(b)

Figure 11. Machine selection of two thresholds for a white blood cell and its nucleus: (a) image of the cell, with 32 gray levels; (b) density histogram, indicating machine-determined thresholds; (c) image partitioned into background (.), nucleus (W), and cytoplasm plus nearby granule ('). Reprinted from Mendelsohn et al [120].

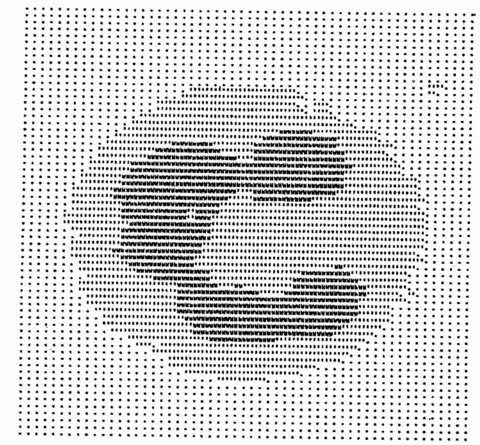

(c)

parison of versions of a scene made at different times, with the aim of detecting significant changes [173]. The overall difference between two pictures p_1 and p_2 can be measured by

$$\iint |p_1 - p_2| \quad \text{or} \quad \iint (p_1 - p_2)^2$$

Algorithms for computing directional derivatives have been discussed above.

Statistical neighborhood comparisons also yield information on change [33, 81, 83]. The gray value at a point $p(x,y)$ is compared to the mean $\bar{p}(x,y) \pm \alpha\sigma\,(x,y)$ over an annular neighborhood $A(x,y)$, where $\sigma(x,y)$ is the standard deviation $\sigma_1^2(x,y) = \iint_{A(x,y)} (p-\bar{p})^2 dxdy$ or mean absolute difference $\sigma_2(x,y) = \iint_{A(x,y)} |p-\bar{p}|\, dxdy$ over the annulus, $\bar{p}(x,y)$ the mean, and α a prespecified factor, usually in the range 0.5 to 1.5. The quantity $(p-\bar{p})/\sigma$ is relatively low at an edge surrounded by other edges, and high at isolated edges or isolated small regions which contrast strongly with their background. Related to these are methods of border definition based on statistical tests of alternative hypotheses about the cumulative gray value distributions of neighboring areas (see below).

Clipping or thresholding may be used conjointly with any of the differencing methods to identify zones of high gradient. Likewise, use

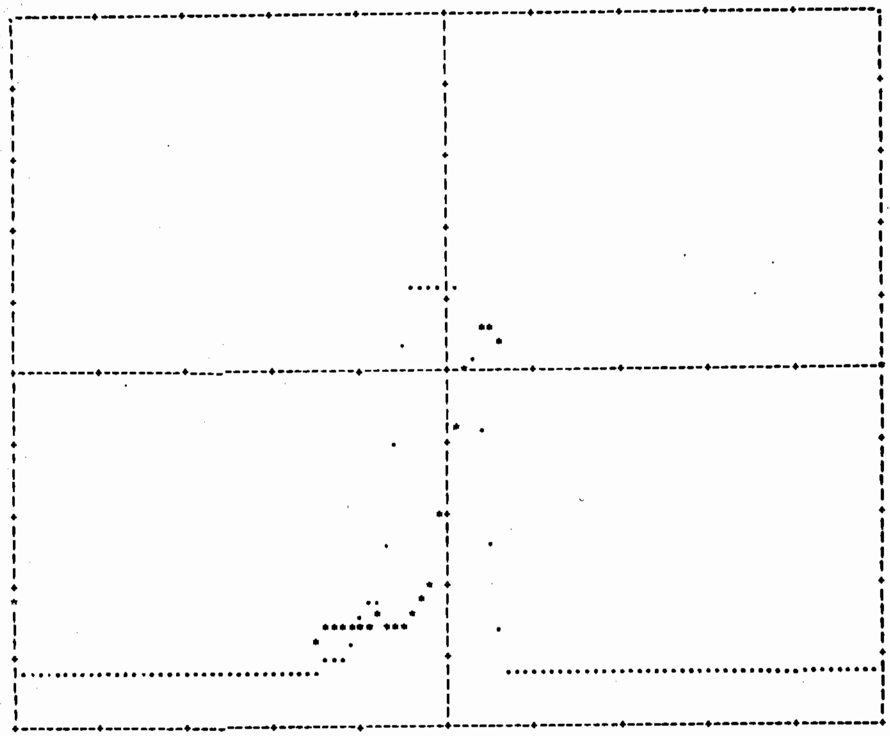

Figure 12a. Edge trace and its derivative at the boundary of the nucleus of the white blood cell of Fig. 11. Mean gray value (*above*) and mean gradient magnitude (*on facing page*) plotted as functions of distance from the boundary. Positive distances correspond to the interior, negative distances to the exterior of the nucleus. * denotes mean density or mean gradient, while · denotes the number of image points at the corresponding distance. The graph of density is actually an edge trace, while the graph of gradient is the corresponding line spread function.

of normalized cross correlation or matched filtering, followed by thresholding, can extract object locations.

Good continuation and closure are subject-dependent, and fortuitous in the preceding approaches, but they are built-in features of tracking

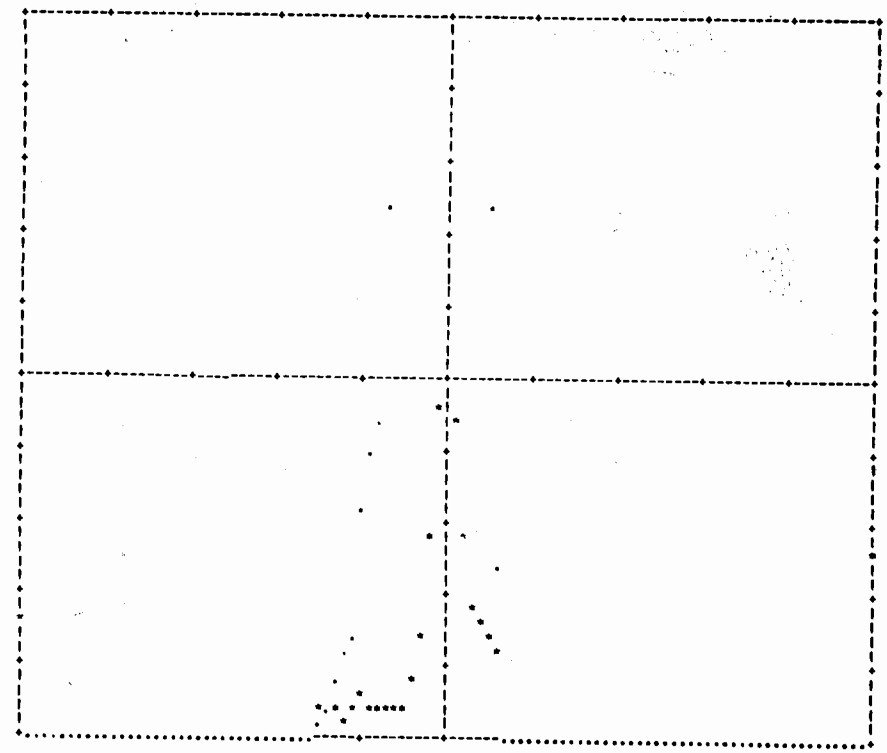

and propagation algorithms. Tracking procedures may be thought of as elementary assemblage or concatenation approaches. The simplest tracking procedures trace around an already-delineated continuous boundary (see above).

It is not difficult to incorporate a look-ahead feature for bridging gaps and disrupting meaningless junctions [62]. Search for a next point can be continued past a gap of a certain length or less; the trace over the gap can proceed in the same direction as the most recent trace around the boundary, matching both slope and curvature, or a fixed angular deviation may be allowed. The computation of gradients and the sequential tracking of the locus of their maxima is a contrast-invariant method

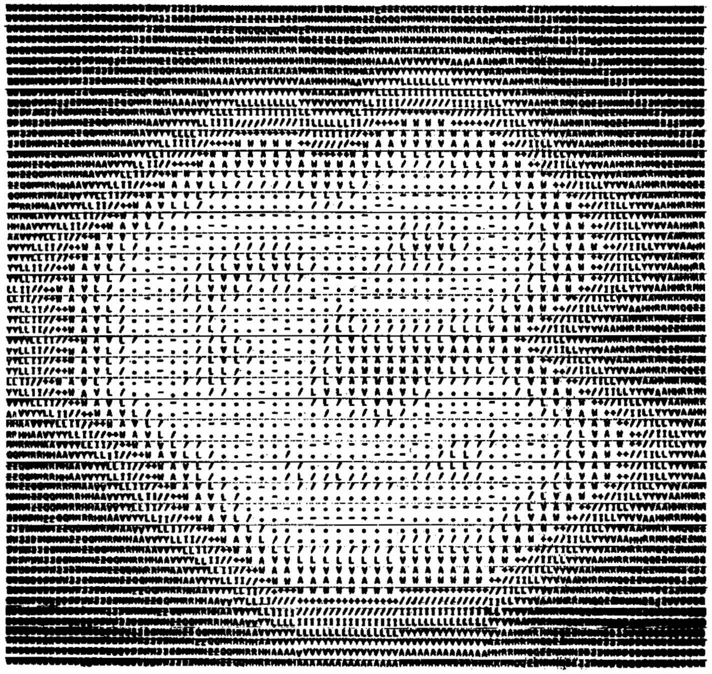

Figure 12b. Distances from the nuclear boundary shown in Fig. 11. The darkness at each point is proportional to distance to the nearest boundary point.

of delineation. The contour of a blood cell nucleus in Fig. 13 was constructed by the following algorithm: The picture is searched for a sharp change in gray value. The gradient threshold for this coarse scan is obtained mechanically from a histogram of gradient magnitudes for the picture. A fine scan mode is then initiated. Two types of tracking motions are involved: (1) local search along the direction of the gradient for a larger gradient magnitude, using a look-around procedure; and (2) movement orthogonal to the maximum gradient to the next candidate point. As the trace proceeds, lists of nodes corresponding to path bifurcations are constructed for later processing [101]; also see [56, 219].

An adaptive line follower which has some principles in common with this has been constructed by Guzman-Arenas [59]. The line follower

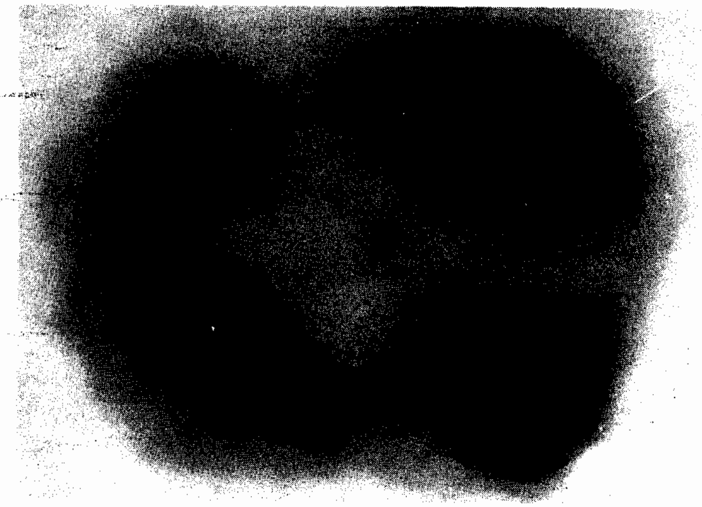

(a)

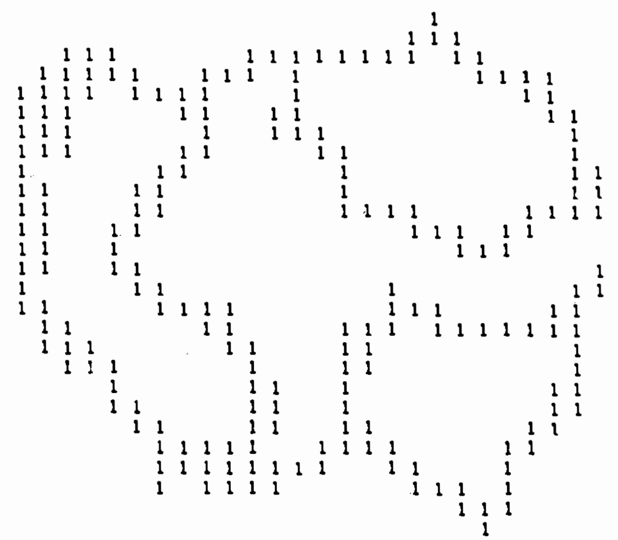

(b)

Figure 13. Outlining by gradient-tracking: (a) photomicrograph of a white blood cell; (b) tracked locus of maximal gradient magnitudes obtained by the algorithm described in the text (tracking imposes continuity on the contours).

consists of three parallel and contiguous rectangles. The innermost is an acceptance box, the others are searching boxes. The widths and length of the boxes are functions of picture noise, length of line already found, and gradient variation. 90% of the points must fall within the acceptance box before it is lengthened. A similar method is described by Krull et al in [104].

Other sequential procedures assemble elementary connected components into complete regions. Geometric assemblage of overlapping runs of 1's and 0's in contiguous scan lines was used early in binary picture processing [20, 57, 209]. More fundamental as an approach to articulation is fragment assemblage based on statistical decisions. The motivation is to construct homogeneous regions by concatenating contiguous picture fragments which have similar gray level or gradient values or similar distribution functions. A three step procedure has been developed for the gray level case using cumulative statistical acceptance criteria ([136]; see also the paper by Muerle in Section III). First, the picture is partitioned into a regular mosaic of sample groups called cells, and the cumulative distribution of gray values is obtained for each cell. Second, pairs of cumulative distributions are compared sequentially using the two-tailed Kolmogorov-Smirnov test for significance of their maximum difference. Third, "similar" fragments are concatenated. The threshold criterion can be tightened as the size of fragments increases, and the mean difference between the cumulative distributions can replace the maximum. The segmentation of the picture is sensitive to choice of starting cells, and to the amount of edge in the picture. In early fragment growth, false acceptances and rejections may occur because of small sample size. The segmentation problem in character recognition is discussed in [25, 75, 101, 150].

Propagation schemes may also be used for segmentation of grayscale pictures. We define two types of skeletons [166]: (1) the endoskeleton, a conventional skeleton of an object or object approximation; and (2) the exoskeleton of a field of view, i.e., the skeleton of the background. The exoskeleton may be computed by a propagation method such as the medial axis transform, or by using a distance transform (or preferably a gray weighted distance transform) and tracking the locus of local maxima. Fig. 14 is based on a 256-level scan of a white cell and a dark granule in the same field of view. Starting from object approxima-

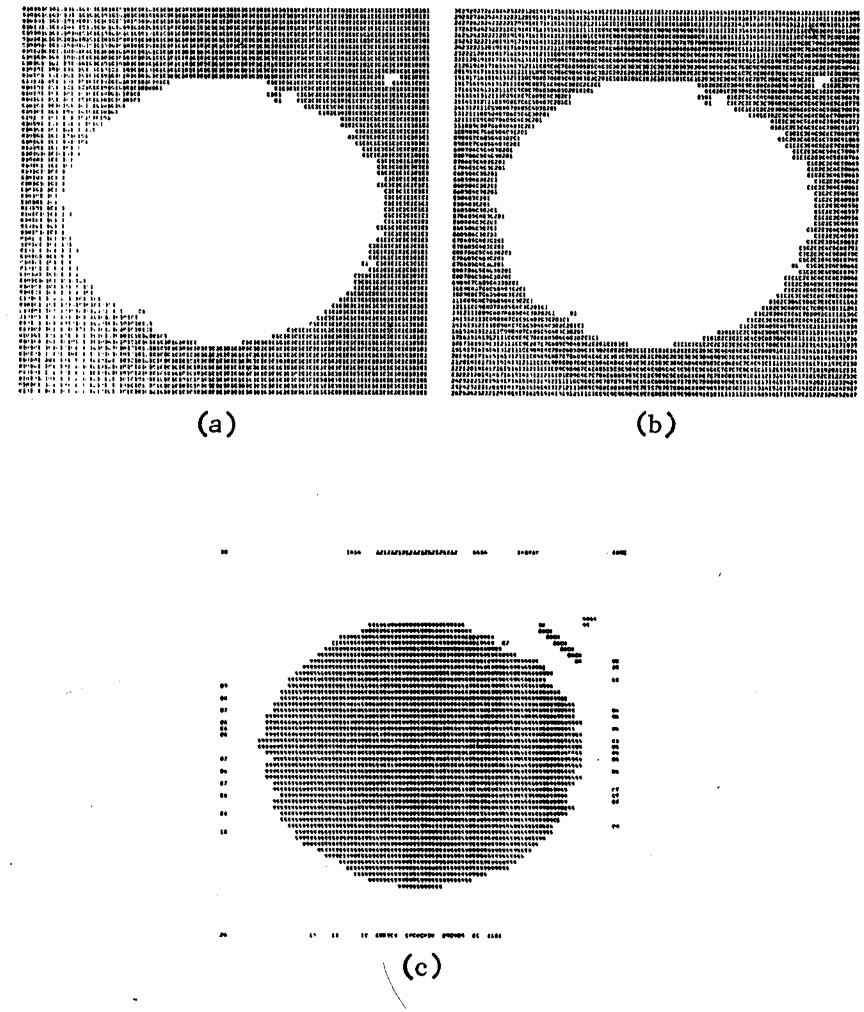

Figure 14. Partitioning the image field by means of exoskeletons. (a) Thresholded version of the field of Fig. 12, containing a blood cell and a nearby granule. Only the entire cell and granule have been delineated. (b) Outward distance transform from these boundaries. (c) Exoskeleton of the field of view. The locus of pseudo-maxima of the distance transform is indicated by the retained distance values.

tions obtained by thresholding "high," an exoskeleton separating granule from cell is derived.

The discussion of syntactic models for concatenating picture elements into objects is beyond the scope of this paper. Representative material can be found in [37, 39, 98, 109, 141, 194].

ACKNOWLEDGEMENTS

The author wishes to express appreciation to the National Institutes of Health for continuing support under a grant from USPHS 1-R01-GM-16913. Computing facilities were made available at the University of Pennsylvania Medical School Computer Facility, under a grant from USPHS RR-515. Appreciation is also expressed to the IEEE Pattern Recognition Group and to NATO for additional assistance.

REFERENCES*

The following collections of papers will be cited by initials:

OCR .... Fischer, G. L., Jr., Pollock, D. K., Radack, B., Stevens, M. E., eds., *Optical Character Recognition,* N.Y.: Spartan, 1962.

OEOIP .... Tippett, J. T., Berkowitz, D.A., Clapp, L. C., Koester, C. J., Vanderburgh, A., Jr., eds., *Optical and Electro-Optical Information Processing,* Cambridge: M.I.T. Press, 1965.

PR .... Uhr, L., ed., *Pattern Recognition,* N.Y.: Wiley, 1966.

PR² .... Kanal, L., ed., *Pattern Recognition,* Washington: Thompson, 1968.

PPR .... Cheng, G. C., Ledley, R. S., Pollock, D. K., Rosenfeld, A., eds., *Pictorial Pattern Recognition,* Washington: Thompson, 1968.

CPR .... *Conference on Pattern Recognition,* Conf. Publ. 42, London: Inst. Elec. Engrs., 1968.

1. Alt, F. L., Digital Pattern Recognition by Moments, in OCR, 153-180.
2. Andrews, H. C., Entropy Considerations in the Frequency Domain, *Proc. IEEE,* **56**, 1968, 113-114.
3. Andrews, H. C., A High Speed Algorithm for the Computer Generation of Fourier Transforms, *IEEE Trans.,* C–17, 1968, 373-375.
4. Andrews, H. C., Automatic Interpretation and Classification of Images by Use of the Fourier Domain, in Grasselli, A., ed., *Automatic Interpretation and Classification of Images,* N.Y.: Academic Press, 1968, 187-198.

*Not all references are cited in the paper.

5. Arcese, A., Menger, P. H., Trombini, E. W., Image Detection through Bipolar Correlation, *IEEE Trans.,* IT–16, in press.
6. Armitage, J. D., Lohmann, A. W., Herrick, R. B., Absolute Contrast Enhancement, *Appl. Opt.,* 4, 1965, 445-451.
7. Arthaber, J., Fundamentals of Spatial Filtering, Rept. TR-960 (AD277551), Diamond Ordnance Fuze Labs., Washington, D. C., June, 1962.
8. Asendorf, R. H., The Remote Reconnaissance of Extraterrestrial Environments, in PPR, 223-238.
9. Attneave, F., Some Informational Aspects of Visual Perception, *Psychol. Rev.,* 61, 1954, 183-193.
10. Attneave, F., Arnoult, M. D., The Quantitative Study of Shape and Pattern Perception, *Psychol. Bull.* 53, 1956, 452-471. Reprinted in PR, 123-141.
11. Ayres, F., Spatial Filtering, M.S. Thesis, Ohio State U., Columbus, Ohio, AD 257470, 1961.
12. Barnes, C. W., Object Restoration in a Diffraction-Limited Imaging System, *J. Opt. Soc. Amer.,* **56**, 1966, 575-578.
13. Billingsley, F. C., Digital Video Processing at JPL, *Electronic Imaging Techniques for Engineering, Laboratory, Astronomical and Other Scientific Measurements,* Redondo Beach, Calif.: S.P.I.E., 1965, paper no. 15.
14. Billingsley, F. C., Processing Ranger and Mariner Photography, *J. SPIE,* 4, 1966, 147-155.
15. Blackman, R. B., Tukey, J. W., *The Measurement of Power Spectra,* N.Y.: Dover, 1958.
16. Bledsoe, W. W., Browning, I., Pattern Recognition and Reading by Machine, *Proc. EJCC,* 1959, 225-232. Reprinted in PR, 301-316.
17. Block, H. D., Nilsson, N. J., Duda, R. O., Determination and Detection of Features in Patterns, in Tou, J. T., Wilcox, R. H., eds., *Computer and Information Sciences,* N.Y.: Spartan, 1964, 75-110.
18. Blum, H., A Transformation for Extracting New Descriptors of Shape, in Wathen-Dunn, W., ed., *Models for the Perception of Speech and Visual Form,* Cambridge: M.I.T. Press, 1967, 362-380.
19. Bomba, J. S., Alpha-Numeric Character Recognition Using Local Operations, *Proc. EJCC,* 1959, 218-224.
20. Butler, J. W., Butler, M. K., Stroud, A., Automatic Analysis of Chromosomes, in Enslein, K., ed., *Data Acquisition and Processing in Biology and Medicine,* N.Y.: Pergamon Press; 3, 1963, 261-275; 4, 1964, 47-57.
21. Calabi, L., Hartnett, W. E., Shape Recognition, Prairie Fires, Convex Deficiencies and Skeletons, *Amer. Math. Monthly,* 75, 1968, 335-342.
22. Casey, R., Nagy, G., Recognition of Printed Chinese Characters, *IEEE Trans.,* EC–15, 1966, 91-101.
23. Charman, W. N., Watrasiewicz, B. M., Mach Effect Associated with Microscopic Images, *J. Opt. Soc. Amer.,* 54, 1964, 791-795.
24. Chow, C. K., An Optimum Character Recognition System Using Decision Functions, *IRE Trans.,* EC–6, 1957, 247-264.
25. Clayden, D. O., Clowes, M. B., Parks, J. R., Letter Recognition and the Segmentation of Running Text, *Info. Control,* **9**, 1966, 246-264.

26. Clowes, M. B., The Use of Multiple Auto-Correlation in Character Recognition, in OCR, 305-318.
27. Cochran, W. T., Cooley, J. W., Favin, D. L., Helms, H. D., Kaenel, R. A., Lang, W. W., Maling, G. C., Jr., Nelson, D. E., Rader, C. M., Welsh, P. D., What is the Fast Fourier Transform?, *Proc. IEEE*, **55**, 1967, 1664-1674.
28. Cooley, J. W., Lewis, P.A.W., Welsh, P. D., Historical Notes on the Fast Fourier Transform, *Proc. IEEE*, **55**, 1967, 1675-1677.
29. Cooley, J. W., Tukey, J. W., An Algorithm for the Machine Calculation of Complex Fourier Series, *Math. Computation*, **19**, 1965, 297-301.
30. Cutrona, L. J., Leith, E. N., Palermo, C. J., Porcello, L. J., Optical Data-Processing and Filtering Systems, *IRE Trans.*, **IT–6**, 1960, 386-400.
31. Courant, R., Hilbert, D., *Methods of Mathematical Physics*, N.Y.: Interscience, 1953.
32. Diamantides, N. D., Correlation Measure of Contrast for Map Matching, *J. Opt. Soc. Amer.*, **58**, 1968, 996-998.
33. Dineen, G. P., Programming Pattern Recognition, *Proc. WJCC*, 1955, 94-100.
34. Dodwell, P. C., Coding and Learning in Shape Discrimination, *Psychol. Rev.*, **68**, 1961, 373-382. Reprinted in PR, 185-194.
35. Doyle, W., Recognition of Sloppy, Hand-Printed Characters, *Proc. WJCC*, 1960, 133-142.
36. Doyle, W., Operations Useful for Similarity-Invariant Pattern Recognition, *J. ACM*, **9**, 1962, 259-267.
37. Eden, M., Halle, M., The Characterization of Cursive Writing, *Proc. Fourth London Symp. on Info. Theory*, London: Butterworth, 1961, 287-299.
38. Efron, E., Image Processing by Digital Systems, *Photogram. Eng.*, **34**, 1968, 1058-1062.
39. Evans, T. G., A Grammar-Controlled Pattern Analyzer, *Proc. IFIP Cong. 68*, Amsterdam: North Holland, 1968, H152-H157.
40. Falconi, O., Limits to which Double Lines, Double Stars, and Discs can be Resolved and Measured, *J. Opt. Soc. Amer.*, **57**, 1967, 987-993.
41. Fiorentini, A., Dynamic Characteristics of Visual Processes, in Wolfe, E., ed., *Progress in Optics 1*, Amsterdam: North Holland, 1961, 255-288.
42. Forsen, G. E., Processing Visual Data with an Automaton Eye, in PPR, 471-502.
43. Freeman, H., On the Encoding of Arbitrary Geometric Configurations, *IEEE Trans.*, **EC–10**, 1961, 260-268.
44. Freeman, H., On the Digital Computer Classification of Geometric Line Patterns, *Proc. Natl. Elect. Conf.*, **18**, 1962, 312-324.
45. Frieden, B. R., Band-Unlimited Reconstruction of Optical Objects and Spectra, *J. Opt. Soc. Amer.*, **57**, 1967, 1013-1019.
46. Frieden, B. R., Optimum Nonlinear Processing of Noisy Images, *J. Opt. Soc. Amer.*, **58**, 1968, 1272-1275.
47. Fryer, W. D., Richmond, G. E., Two-Dimensional Spatial Filtering and Computers, *Proc. Natl. Elect. Conf.*, **18**, 1962, 529-535.
48. Gabor, D., Light and Information, in Wolfe, E., ed., *Progress in Optics 1*, Amsterdam: North Holland, 1961, 111-153.
49. Gabor, D., Character Recognition by Holography, *Nature*, **208**, 1965, 422.

50. Gabor, D., Information Theory in Electron Microscopy, *Lab. Investig.*, 14, 1965, 801-807.
51. Gerardin, L. A., Flament, J., Geometrical Pattern Feature Extraction by Projection on Haar Orthonormal Basis, in Walker, D. E., Norton, L. M., eds., *Proc. Intl. Joint Conf. on Artif. Intell.*, Washington, D. C., May, 1969, 65-77. Preprint.
52. Gilmore, H. F., Models of The Point Spread Function of Photographic Emulsions Based on a Simplified Diffusion Calculation, *J. Opt. Soc. Amer.*, **57**, 1967, 75-80.
53. Goldmark, P. C., Hollywood, J. M., A New Technique for Improving the Sharpness of Television Pictures, *Proc. IRE*, **39**, 1951, 1314-1322.
54. Graham, D. N., Image Transmission by Two-Dimensional Contour Coding, *Proc. IEEE*, **55**, 1967, 336-346.
55. Graham, R. E., Snow Removal—a Noise Stripping Process for Picture Signals, *IRE Trans.*, **IT–8**, 1962, 129-144.
56. Greanias, E. C., Meagher, P. F., Norman, R. J., Essinger, P., The Recognition of Handwritten Numerals by Contour Analysis, *IBM J. Res. Dev.*, 7, 1963, 14-21.
57. Grimsdale, R. L., Sumner, F. H., Tunis, C. J., Kilburn, T., A System for the Automatic Recognition of Patterns, *Proc. IEE*, **106**, 1959, 210-221. Reprinted in PR, 317-338.
58. Groner, G. F., Real-Time Recognition of Handprinted Symbols, in PR^2, 103-108.
59. Guzman-Arenas, A., Some Aspects of Pattern Recognition by Computer, Rept. MAC-TR-37 (AD 656041), Project MAC, M.I.T., Cambridge, Mass., Feb., 1967.
60. Haar, A., Zur Theorie der Orthogonal Functionen Systema, *Math. Ann.*; I, 69, 1912, 331-371; II, **70**, 1912, 38-53.
61. Hake, H. W., Form Discrimination and the Invariance of Form, in PR, 142-173.
62. Hankley, W. J., Tou, J. T., Automatic Fingerprint Interpretation and Classification via Contextual Analysis and Topological Coding, in PPR, 411-456.
63. Harley, T. J., Jr., Electronic Correlation Techniques for Change Detection, Rept. 9034-F (AD276746), Philco Corp., Blue Bell, Pa., Feb., 1962.
64. Harmon, L. D., A Line-Drawing Pattern Recognizer, *Proc. WJCC*, 1960, 351-364.
65. Harmon, L. D., Knowlton, K. C., Picture Processing by Computer, *Science*, 164, 1969, 19-29.
66. Harris, J. L., Resolving Power and Decision Theory, *J. Opt. Soc. Amer.*, **54**, 1964, 606-611.
67. Harris, J. L., Diffraction and Resolving Power, *J. Opt. Soc. Amer.*, **54**, 1964, 931-936.
68. Harris, J. L., Image Evaluation and Restoration, *J. Opt. Soc. Amer.*, **56**, 1966, 569-574.
69. Hawkins, J. K., Photographic Techniques for Extracting Image Shapes, *Phot. Sci. Eng.*, 8, 1964, 329-335.
70. Hawkins, J. K., Parallel Electro-Optical Picture Processing, in PPR, 373-385.
71. Hawkins, J. K., Elerding, G. T., Bixby, K. W., Haworth, P. A., Automatic Shape Detection for Programmed Terrain Classification, *Filmed Data and Computers*, Redondo Beach, Calif.: S.P.I.E., 1966, paper no. 16.

72. Hawkins, J. K., Munsey, J. C., Automatic Photo Reading, *Photogram. Eng.*, **29**, 1963, 632-640.
73. Hawkins, J. K., Munsey, C. J., Image Processing by Electro-Optical Techniques, *J. Opt. Soc., Amer.*, **57**, 1967, 914-918.
74. Helstrom, C. W., Image Restoration by the Method of Least Squares, *J. Opt. Soc. Amer.*, **57**, 1967, 297-303.
75. Hennis, R. B., Recognition of Unnurtured Characters in a Multifont Environment, in PR², 79-100.
76. Higgins, G. C., Wolfe, R. N., The Relation of Definition to Sharpness and Resolving Power in Photographic Systems, *J. Opt. Soc. Amer.*, **45**, 1955, 121-129.
77. Highleyman, W. H., An Analog Method for Character Recognition, *IRE Trans.*, EC–**10**. 1961, 501-512.
78. Highleyman, W. H., Linear Decision Functions with Application to Pattern Recognition, in OCR, 1962, 249-286.
79. Hodges, D., Spark Chamber Film Measuring Using the CHLOE System, in PPR, 199-206.
80. Holeman, J. M., Holographic Character Reader, in PR², 63-78.
81. Holmes, W. S., Automatic Photointerpretation and Target Location, *Proc. IEEE*, **54**, 1966, 1679-1686.
82. Holmes, W. S., Leland, H. R., Muerle, J. L., Recognition of Mixed-Font Imperfect Characters, in OCR, 213-226.
83. Holmes, W. S., Leland, H. R., Richmond, G. E., Design of a Photointerpretation Automaton, *Proc. FJCC*, 1962, 27-35.
84. Horwitz, L. P., Shelton, G. L., Jr., Pattern Recognition Using Autocorrelation, *Proc. IRE*, **49**, 1961, 175-185.
85. Hough, P.V.C., Powell, B. W., A Method for Faster Analysis of Bubble Chamber Photographs, in *Proc. of an International Conf. on Instrumentation for High-Energy Physics*, N.Y.: Interscience, 1961, 242-245.
86. Hu, M. K., Visual Pattern Recognition by Moment Invariants, *IRE Trans.*, IT–8, 1962, 179-187.
87. Huang, T. S., Tretiak, O. J., Research in Picture Processing, in OEOIP, 45-57.
88. Huang, T. S., Tretiak, O. J., Prasada, B., Yamaguchi, Y., Design Considerations in PCM Transmission of Low-Resolution Monochrome Still Pictures, *Proc. IEEE*, **55**, 1967, 331-335.
89. Izzo, N. F., Coles, W., Blood-Cell Scanner Identifies Rare Cells, *Electronics*, **35**, April 27, 1962, 52-57.
90. Janssen, T. J., Kozlowski, J. C., Luther, A. J., Real-Time Digital Subtraction and Enhancement of Video Pictures, *J. SPIE*, **6**, 1968, 120-124.
91. Jenkins, G. M., General Considerations in the Estimation of Spectra, *Technometrics*, **3**, 1961, 138-166.
92. Jones, C. M., Kellaher, J. F., Dillard, J. M., Bernstein, S. L., Fourier Transform Methods for Pattern Recognition, AFCRL, Bedford, Mass., AD 285794, July, 1962.
93. Jones, R. C., On the Point and Line Spread Functions of Photographic Images, *J. Opt. Soc. Amer.*, **48**, 1958, 934-937.

94. Julesz, B., Problems of Pattern Recognition and Perceptual Psychology, in PR², 143-154.
95. Kaizer, H., A Quantification of Textures on Aerial Photographs, AD 69484, Optical Res. Lab., Boston U., Boston, Mass., June, 1955.
96. Kamentsky, L. A., Liu, C. N., Computer-Automated Design of Multifont Print Recognition Logic, *IBM J. Res., Dev.*, 7, 1963, 2-13.
97. Kazmierczak, H., Steinbuch, K., Adaptive Systems in Pattern Recognition, *IEEE Trans.*, EC–**12**, 1963, 822-835.
98. Kirsch, R. A., Computer Interpretation of English Text and Picture Patterns, *IEEE Trans.*, EC–13, 1964, 363-376.
99. Kirsch, R. A., Cahn, L., Ray, C., Urban, G. H., Experiments in Processing Pictorial Information with a Digital Computer, *Proc. EJCC*, 1957, 221-229.
100. Kohler, R., Howell, H., Photographic Image Enhancement by Superposition of Multiple Images, *Phot. Sci. Eng.*, 7, 1963, 241-245.
101. Kovalevsky, V. A., Sequential Optimization in Pattern Recognition and Pattern Description, *Proc. IFIP Cong. 68*, Amsterdam: North-Holland, 1968, I146-I151.
102. Kovasznay, L. S. G., Joseph, H. M., Processing of Two-Dimensional Patterns by Scanning Techniques, *Science*, 118, 1953, 475-477.
103. Kovasznay, L. S. G., Joseph, H. M., Image Processing, *Proc. IRE*, 43, 1955, 560-570.
104. Krull, F. N., Foote, J. E., A Line Scanning System Controlled from an On-Line Console, *Proc. FJCC*, 1964, 397-410.
105. Ledley, R. S., Jacobsen, J., Belson, M., BUGSYS: A Programming System for Picture Processing—Not for Debugging, *Comm. ACM*, **9**, 1966, 79-84.
106. Ledley, R. S., Ruddle, F. H., Wilson, J. B., Belson, M., Albarran, J., The Case of the Touching and Overlapping Chromosomes, in PPR, 87-97.
107. Levinson, N., The Wiener RMS (Root Mean Error) in Filter Design and Prediction, in Wiener, N., *Extrapolation, Interpolation, and Smoothing of Stationary Time Series with Engineering Applications*, N.Y.: Wiley, 1949, 129-148.
108. Linfoot, E. H., *Fourier Methods in Optical Image Evaluation*, N.Y.: Focal Press, 1964.
109. Lipkin, L. E., Watt, W. C., Kirsch, R. A., The Analysis, Synthesis, and Description of Biological Images, *Ann. N.Y. Acad. Sci.*, 128, 1966, 984-1012.
110. Liu, C. N., A Programmed Algorithm for Designing Multifont Character Recognition Logics, *IEEE Trans.*, EC–13, 1964, 586-593.
111. Lohmann, A. W., Paris, D. P., Computer Generated Spatial Filters for Coherent Optical Data Processing, *Appl. Opt.*, 7, 1968, 651-655.
112. Mason, S. J., Clemens, J. K., Character Recognition in an Experimental Reading Machine for the Blind, in Kolers, P. A., Eden, M., eds., *Recognizing Patterns*, Cambridge: M.I.T. Press, 1968, 155-167.
113. Mayall, B. H., Metz, C. E., Mendelsohn, M. L., Evaluation of Enhancement as Applied to Digital Images of Human Chromosomes, *Quart. Bull. Amer. Assn. Physicists in Med.*, **3**, 1969, 37.
114. McCormick, B. H., The Illinois Pattern Recognition Computer—ILLIAC III, *IEEE Trans.*, EC–**12**, 1963, 791-813.

115. McCutchen, C. W., Superresolution in Microscopy and the Abbe Resolution Limit, *J. Opt. Soc. Amer.*, **57**, 1967, 1190-1192.
116. McGlamery, B. L., Restoration of Turbulence-Degraded Images, *J. Opt. Soc. Amer.*, **57**, 1967, 293-297.
117. McLaughlin, J. A., Raviv, J., Nth Order Autocorrelations in Pattern Recognition, *Info. Control*, **12**, 1968, 121-142.
118. Meltzer, B., Searle, N. H., Brown, R., Numerical Specification of Biological Form, *Nature*, **216**, 1967, 32-36.
119. Mendelsohn, M. L., Mayall, B. H., Prewitt, J. M. S., Approaches to the Automation of Chromosome Analysis, in Ramsey, D., ed., *Image Processing in Biological Science*, Los Angeles: U. of Calif. Press, 1969, 119-136.
120. Mendelsohn, M. L., Mayall, B. H., Prewitt, J. M. S., Bostrom, R. C., Holcomb, W. G., Digital Transformation and Computer Analysis of Microscopic Images, in Barer, R., Cosslett, V. E., eds., *Advances in Optical and Electron Microscopy 2*, London: Academic Press, 1968, 77-150.
121. Menzel, E., Weingartner, I., Image Formation and Nonlinear Transfer, *J. Opt. Soc. Amer.*, **57**, 1967, 842-843.
122. Mermelstein, P., Eden, M., Experiments in Computer Recognition of Connected Handwritten Words, *Info. Control*, **7**, 1964, 255-270.
123. Mertz, P., Gray, F., A Theory of Scanning and its Relation to the Characteristics of the Transmitted Signal in Telephotography and Television, *Bell Syst. Tech. J.*, **13**, 1934, 464-515.
124. Meyers, P. H., Becker, H. C., Sweeney, J. W., Nice, C. M., Jr., Nettleton, W. J., Jr., Evaluation of a Computer-Retrieved Radiographic Image, *Radiology*, **81**, 1963, 201-206.
125. Middleton, D., *An Introduction to Statistical Communication Theory*, N.Y.: McGraw Hill, 1960.
126. Minot, O. N., Counting and Outlining of Two-Dimensional Patterns by Digital Computer, Rept. TM-414, U.S. Naval Electronic Lab., San Diego, Calif., Aug., 1960.
127. Minot, O. N., Automatic Devices for Recognition of Visible Two-Dimensional Patterns: a Survey of the Field, Rept. 1050, U.S. Naval Electronic Lab., San Diego, Calif., June, 1961.
128. Minsky, M. L., Heuristic Aspects of the Artificial Intelligence Problem, Rept. 34-55, AD 236885, Lincoln Lab., M.I.T., Cambridge, Mass., Dec., 1956.
129. Minsky, M. L., Steps toward Artificial Intelligence, in Feigenbaum, E. A., Feldman, J., eds., *Computers and Thought*, N.Y.: McGraw-Hill, 1963, 406-450.
130. Minsky, M. L., Papert, S., *Perceptrons: an Introduction to Computational Geometry*, Cambridge: M.I.T. Press, 1969.
131. Montanari, U., Continuous Skeletons from Digitized Images, *J. ACM*, **16**, 1969, 534-549 (see also **15**, 1968, 600-624.)
132. Montanari, U., A Note on Minimal Length Polygonal Approximation to a Digitized Contour, *Comm. ACM*, **13**, 1970, 41-47.
133. Montgomery, W. D., Broome, P. W., Spatial Filtering, *J. Opt. Soc. Amer.*, **52**, 1962, 1259-1275.

134. Moore, G. A., Automatic Scanning and Computer Processes for the Quantitative Analysis of Micrographs and Equivalent Subjects, in PPR, 275-326.
135. Mueller, P. F., Reynolds, G. O., Image Restoration by Removal of Random-Media Degradations, *J. Opt. Soc. Amer.*, **57**, 1967, 1338-1344.
136. Muerle, J. L., Allen, D. C., Experimental Evaluation of Techniques for Automatic Segmentation of Objects in a Complex Scene, in PPR, 3-13.
137. Munson, J. H., The Recognition of Hand-Printed Text, in PR^2, 115-140.
138. Nadler, M., An Analog-Digital Character Recognition System, *IEEE Trans.*, **EC-12**, 1963, 814-821.
139. Nagy, G., State of the Art in Pattern Recognition, *Proc. IEEE*, **56**, 1968, 836-862.
140. Narasimhan, R., Labeling Schemata and Syntactic Descriptions of Pictures, *Info. Control*, **7**, 1964, 151-179.
141. Narasimhan, R., Syntax-Directed Interpretation of Classes of Pictures, *Comm. ACM*, **9**, 1966, 166-173.
142. Narasimhan, R., Fornango, J. P., Some Further Experiments in the Parallel Processing of Pictures, *IEEE Trans.*, **EC-13**, 1964, 748-750.
143. Nathan, R., Picture Enhancement for the Moon, Mars, and Man, in PPR, 239-266.
144. Nilsson, N. J., *Learning Machines*, N.Y.: McGraw-Hill, 1965.
145. Nilsson, N. J., Adaptive Pattern Recognition: a Survey, in Ostreicher, H. L., Moore, D. R., eds., *Cybernetic Problems in Bionics; Bionics Symp. 1966*, N.Y.: Gordon and Breach, 1968, 103-146.
146. Ogawa, H., Isomichi, Y., Optimum Spatial Filter and Uncertainty, *Info. Control*, **14**, 1969, 180-216.
147. Oppenheim, A. V., Schafer, R. W., Stockham, T. G., Jr., Nonlinear Filtering of Multiplied and Convolved Signals, *Proc. IEEE*, **56**, 1968, 1264-1291.
148. Papoulis, A., Optical Systems, Singularity Functions, Complex Hankel Transforms, *J. Opt. Soc. Amer.*, **57**, 1967, 207-213.
149. Papoulis, A., *Systems and Transforms with Applications in Optics*, N.Y.: McGraw-Hill, 1969.
150. Parks, J. R., Elliott, J. R., Cowin, G., Simulation of an Alphanumeric Character Recognition System for Unsegmented Low Quality Print, in CPR, 95-105.
151. Parzen, E., Mathematical Considerations in the Estimation of Spectra, *Technometrics*, **3**, 1961, 167-190.
152. Pease, M. C., An Adaptation of the Fast Fourier Transform for Parallel Processing, *J. ACM*, **15**, 1968, 252-264.
153. Perrin, F. H., Methods of Appraising Photographic Systems, *J. Soc. Motion Pict. TV Eng.*; I. Historical Review, **69**, 1960, 151-156; II. Manipulation and Significance of Sine-Wave Response Function, **69**, 1960, 239-249.
154. Petersen, D. J., Middleton, D., Reconstruction of Multidimensional Stochastic Fields from Discrete Measurements of Amplitude and Gradient, *Info. Control*, **7**, 1964, 445-476.
155. Petersen, D. P., Middleton, D., Sampling and Reconstruction of Wave-Number-Limited Functions in n-Dimensional Euclidean Spaces, *Info. Control*, **5**, 1962, 279-323.
156. Pfaltz, J. L., Rosenfeld, A., Computer Representation of Planar Regions by their Skeletons, *Comm. ACM*, **10**, 1967, 119-125.

157. Pfaltz, J. L., Snively, J. W., Jr., Rosenfeld, A., Local and Global Picture Processing by Computer, in PPR, 353-372.
158. Philbrick, O., Shape Description with the Medial Axis Transformation, in PPR, 395-407.
159. Pike, W. S., Some Television Image Enhancement Techniques, *Ann. N.Y. Acad. Sci.*, **97**, 1962, 395-407.
160. Pizer, S. M., Vetter, H. G., Perception and Processing of Medical Radioisotope Scans, in PPR, 147-156.
161. Potsaid, M. S., Swanlund, C. D., King, G. E., Neuberger, A., A Computer Analysis of Radiographs, in *Lippincott's Medical Science*, 17, 1966, 35-43.
162. Prewitt, J. M. S., The Selection of Sampling Rate for Digital Sampling, *IEEE Trans.*, **BME–12**, 1965, 14-21.
163. Prewitt, J. M. S., Mayall, B. H., Mendelsohn, M. L., Pictorial Data Processing Methods in Microscopy, *Filmed Data and Computers*, Redondo Beach, Calif.: S.P.I.E., June, 1966, paper no. 15.
164. Prewitt, J. M. S., Mendelsohn, M. L., The Analysis of Cell Images, *Ann. N.Y. Acad. Sci.*, **128**, 1966, 1035-1053.
165. Prewitt, J. M. S., Mendelsohn, M. L., A General Approach to Image Analysis by Parameter Extraction, in *Proc. of a Conf. on the Use of Computers in Radiology*, U. of Missouri, 1966, A2-A41.
166. Prewitt, J. M. S., Prog. Rept., Digital Computers and Scanning Cytophotometry, Dept. of Radiology, U. of Pa., Philadelphia, Pa., 1965.
167. Prosser, R. T., A Multidimensional Sampling Theorem, *J. Math Anal. Appl.*, **16**, 1966, 574-584.
168. Rabinow, J., Developments in Character Recognition Machines at Rabinow Engineering Company, in OCR, 27-50.
169. Rabinowitz, G., Current Status of Automatic Scanning at Brookhaven National Laboratory and Columbia University, in PPR, 159-174.
170. Rao, C. R., *Advanced Statistical Methods in Biometric Research*, N.Y.: Wiley, 1962.
171. Rao, U. V. G., Jain, V. K., Gaussian and Exponential Approximation of the Modulation Transfer Function, *J. Opt. Soc. Amer.*, **57**, 1967, 1159-1160.
172. Ratliff, F., *Mach Bands: Quantitative Studies on Neural Networks in the Retina*, San Francisco: Holden-Day, 1965.
173. Rau, J. E., Detection of Differences in Real Distributions, *J. Opt. Soc. Amer.*, **56**, 1966, 1490-1494.
174. Rhodes, J., Analysis and Synthesis of Optical Images, *Amer. J. Phys.*, **21**, 1953, 337-343.
175. Roberts, L. G., Picture Coding using Pseudorandom Noise, *IRE Trans.*, **IT–8**, 1962, 145-154.
176. Roberts, L. G., Recent Developments in Optical Character Recognition at M.I.T., in OCR, 209-212.
177. Roberts, L. G., Machine Perception of Three-Dimensional Solids, in OEOIP, 159-197.
178. Roberts, L. G., Pattern Recognition with an Adaptive Network, in PR, 295-300.
179. Root, W. L., Davenport, W. B., *An Introduction to the Theory of Random Signals and Noise*, N.Y.: McGraw-Hill, 1958.

180. Rosenblatt, F., *Principles of Neurodynamics*, N.Y.: Spartan, 1962.
181. Rosenblatt, F., A Comparison of Several Perceptron Models, in Yovits, M. C., et al, eds., *Self-Organizing Systems*, N.Y.: Spartan, 1962, 463-484.
182. Rosendahl, G. R., Retrieval of Optical Performance Functions from an Edge Trace with Rigid Control by Least Squares, *Photooptical Systems Evaluation Seminar*, Redondo Beach, Calif.: S.P.I.E., 1967, XII 1-12.
183. Rosenfeld, A., *Picture Processing by Computer*, N.Y.: Academic Press, 1969.
184. Rosenfeld, A., Huang, H. K., Schneider, V. B., An Application of Cluster Detection to Text and Picture Processing, *IEEE Trans.*, **IT–15**, 1969, 672-681.
185. Rosenfeld, A., Pfaltz, J. L., Sequential Operations in Digital Picture Processing, *J. ACM*, 13, 1966, 471-494.
186. Rushforth, C. K., Harris, R. W., Restoration, Resolution, and Noise, *J. Opt. Soc. Amer.*, **58**, 1968, 539-545.
187. Rutovitz, D., Data Structures for Operations on Digital Images, in PPR, 105-133.
188. Schreiber, W. F., Picture Coding, *Proc. IEEE*, **55**, 1967, 320-330.
189. Sebestyen, G. S., *Decision-Making Processes in Pattern Recognition*, N.Y.: Macmillan, 1962.
190. Sebestyen, G. S., Machine-Aided Reconnaissance and Photointerpretation, *J. SPIE*, **2**, 1964, 89-92.
191. Selfridge, O. G., Pandemonium: a Paradigm for Learning, in PR, 339-348.
192. Selfridge, O. G., Neisser, U., Pattern Recognition by Machine, in Feigenbaum, E. A., Feldman, J., eds., *Computers and Thought*, N.Y.: McGraw-Hill, 1963, 237-250.
193. Selzer, R. H., Digital Computer Processing of X-Ray Photographs, in Enslein, K., ed., *Data Acquisition and Processing in Biology and Medicine* 5, N.Y.: Pergamon Press, 1968, 309-325.
194. Shaw, A. C., A Formal Picture Description Scheme as a Basis for Picture Processing Systems, *Info. Control*, 14, 1969, 9-52.
195. Slepian, D., Linear Least-Squares Filtering of Distorted Images, *J. Opt. Soc. Amer.*, **57**, 1967, 918-922.
196. Slepian, D., Restoration of Photographs Blurred by Image Motion, *Bell Syst. Tech. J.*, **46**, 1967, 2353-2362.
197. Slepian, D., Pollack, H. O., Landau, H. S., Prolate Spheroidal Wave Functions, Fourier Analysis, and Uncertainty, *Bell Syst. Tech. J.*, **40**, 1961, 43-84; **41**, 1962, 1295-1336.
198. Smith, F. W., Wright, M. H., Automatic Ship Photointerpretation by the Method of Moments, Rept. SESW-M1169, Sylvania Electronic Systems, Mountain View, Calif., Nov., 1967.
199. Sneath, P.H.A., A Method for Curve Seeking from Scattered Points, *Comp. J.*, **8**, 1966, 383-391.
200. Sneddon, I., Finite Hankel Transforms, *Phil. Mag.*, **37**, 1946, 17-25.
201. Spinrad, R. J., Machine Recognition of Hand Printing, *Info. Control*, **8**, 1965, 124-142.
202. Stevens, M. E., Automatic Character Recognition: a State-of-the-Art Report, Tech. Note 112, PB 161613, Nat. Bur. Standards, Washington, D.C., 1961.
203. Stevens, M. E., Abstract Shape Recognition by Machine, *Proc. EJCC*, 1961, 332-351.

204. Stock, R. M., Deener, J. J., A Real-time Input Preprocessor for a Pattern Recognition Computer, *Proc. IEEE Computer Conf.*, 1967, 149-152.
205. Stuart, R. D., *An Introduction to Fourier Analysis*, London: Methuen, 1961.
206. Sugiura, T., Higashiuwatoko, T., A Method for the Recognition of Japanese Hiragana Characters, *IEEE Trans.*, IT–14, 1968, 226-233.
207. Swoboda, W., Gerdes, J. W., A System for Demonstrating the Effects of Changing Background on Automatic Target Recognition, in PPR, 33-44.
208. Teitelman, W., Real Time Recognition of Hand-Drawn Characters, *Proc FJCC*, 1964, 559-575.
209. Tolles, W., Mansberg, H. P., Size and Shape Determination in Scanning Microscopy, *Ann. N.Y. Acad. Sci.*, **97**, 1962, 516-526.
210. Tomita, S., Noguchi, S., Recognition of Handwritten Katakana Characters *Electronics and Communications in Japan, J. Inst. Elec. Comm. Eng. Japan*, **50**, 1967, 174-183.
211. Tou, J.T., Heydorn, R. P., Some Approaches to Optimum Feature Extraction, in Tou., J. T., ed., *Computer and Information Sciences—II*, N.Y.: Academic Press, 1967, 57-89.
212. Trabka, E. A., Roetling, P. G., Image Transformations for Pattern Recognition using Incoherent Illumination and Bipolar Aperture Masks, *J. Opt. Soc. Amer.*, **54**, 1964, 1242-1252.
213. Trabka, E. A., Roetling, P. G., Shape Detection Using Incoherent Illumination, *J. Opt. Soc. Amer.*, **57**, 1967, 108-110.
214. Tranter, C. J., *Integral Transforms in Mathematical Physics*, London: Methuen, 1951.
215. Tsujiuchi, J., Correction of Optical Images by Compensation of Aberrations and by Spatial Frequency Filtering, in Wolfe, E., ed., *Progress in Optics* 2, N.Y.: Wiley, 1963, 131-180.
216. Tukey, J. W., Discussion Emphasizing the Connection between Analysis of Variance and Spectrum Analysis, *Technometrics*, 3, 1961, 191-219.
217. Uhr, L., Vossler, C., A Pattern Recognition Program that Generates, Evaluates, and Adjusts its Own Operators, *Proc. WJCC*, 1961, 555-569. Reprinted in PR, 349-364.
218. Unger, S. H., A Computer Oriented toward Spatial Problems, *Proc. IRE*, **46**, 1958, 1744-1750.
219. Unger, S. H., Pattern Detection and Recognition, *Proc. IRE*, **47**, 1959, 1737-1752.
220. Vander Lugt, A., Signal Detection by Complex Spatial Filtering, *IEEE Trans.*, **IT–10**, 1964, 139-145.
221. Vander Lugt, A., The Effects of Small Displacements of Spatial Filters, *Appl. Opt.*, **6**, 1967, 1221-1225.
222. Vander Lugt, A., A Review of Optical Data-Processing Techniques, *Optica Acta*, **15**, 1968, 1-33.
223. Vandar Lugt, A., Mitchel, R. H., Technique for Measuring Modulation Transfer Functions of Recording Media, *J. Opt. Soc. Amer.*, **57**, 1957, 372-379.
224. Vander Lugt, A., Rotz, F. B., Klooster, A., Jr., Character Reading by Optical Spatial Filtering, in OEOIP, 125-141.
225. van der Pol, B., Smoothing and "Unsmoothing," in Kac, M., ed., *Probability and Related Topics in Physical Science 1*, London: Interscience, Appendix III.

226. Vetter, H. G., Restoration of Biological Images using Limited Sampling, *Physics in Med. and Biol.*, 14, 1969, 417-430.
227. Walsh, J. L., Properties of Haar's System of Orthogonal Functions, *Math. Ann.*, **90**, 1923, 38-45.
228. Watanabe, S., Lambert, P. F., Kulikowski, C. A., Buxton, J. L., Walker, R., Evaluation and Selection of Variables in Pattern Recognition, in Tou, J. T., ed., *Computer and Information Sciences—II*, N.Y.: Academic Press, 1967, 91-122.
229. Watts, T. L., Scanning and Measuring Photographs of Bubble Chamber Tracks Using a Computer Controlled Line Segment ("PEPR"), in PPR, 207-220.
230. White, B. W., The Computer as a Patttrn Generator for Perceptual Research, *Behav. Sci.*, 6, 1961, 252-259.
231. White, H. S., DAPR—Digital Automatic Pattern Recognition for Bubble Chambers, in PPR, 175-199.
232. Wolfe, R. N., Eisen, F. C., Psychometric Evaluation of the Sharpness of Photographic Reproductions, *J. Opt. Soc., Amer.*, 43, 1963, 914-922.
233. Wong, E., Two-dimensional Random Fields and Representation of Images, *SIAM J. Appl. Math.*, 16, 1968, 756-770.
234. Wonnacott, T. H., Spectral Analysis Combining a Bartlett Window with an Associated Inner Window, *Technometrics*, 3, 1961, 235-243.
235. Wood, R. C., On Optimum Quantization, *IEEE Trans.*, **IT–15**, 1969, 248-252.
236. Zadeh, L. A., Fuzzy Sets, *Info. Control*, 8, 1965, 338-353.
237. Zemanian, A. H., *Generalized Integral Transformations*, N.Y.: Interscience, 1968.